Article

Immunity

# Small intestinal resident eosinophils maintain gut homeostasis following microbial colonization

## Graphical abstract

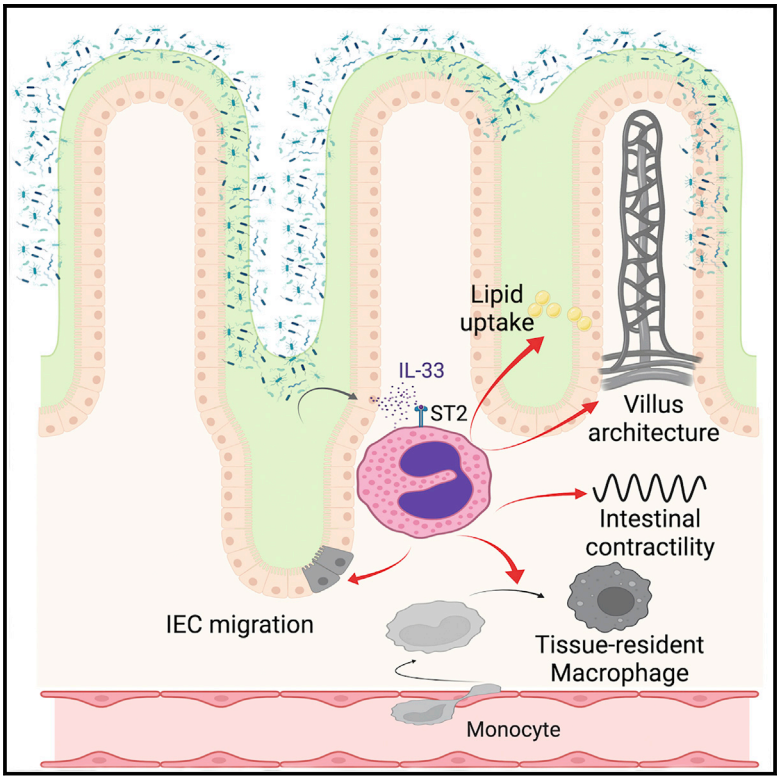


## Highlights

- Colonization of GF mice activates small intestinal eosinophils
- Whole-mount microscopy of SI reveals villus blunting in the absence of eosinophils
- Loss of eosinophils leads to reduced numbers of mature intestinal macrophages
- Transfer of bone-marrow-derived eosinophils rescues the loss of intestinal homeostasis

## Authors

Aline Ignacio, Kathleen Shah, Jeremiah Bernier-Latmani, ..., Tatiana V. Petrova, Nicola L. Harris, Kathy D. McCoy

## Correspondence

nicola.harris@monash.edu (N.L.H.), kathy.mccoy@ucalgary.ca (K.D.M.)

## In brief

Eosinophils are resident cells found in high numbers in the small intestine. Ignacio et al. reveal that in response to microbial colonization, eosinophils sense the IL-33 released by epithelial cells to maintain the integrity of the intestinal villi, epithelial cell turnover, intestinal barrier function, and recruitment of mature macrophages to maintain homeostasis.

Ignacio et al., 2022, Immunity *55*, 1–18
July 12, 2022 
https://doi.org/10.1016/j.immuni.2022.05.014

CellPress

Please cite this article in press as: Ignacio et al., Small intestinal resident eosinophils maintain gut homeostasis following microbial colonization, Immunity (2022), https://doi.org/10.1016/j.immuni.2022.05.014

Immunity

CellPress

Article

# Small intestinal resident eosinophils maintain gut homeostasis following microbial colonization

Aline Ignacio,[1,14] Kathleen Shah,[2,3,14] Jeremiah Bernier-Latmani,[4,14] Yasmin Köller,[5] Gillian Coakley,[6] Mati Moyat,[2,6] Romain Hamelin,[7] Florence Armand,[7] Nick C. Wong,[8] Hena Ramay,[9] Carolyn A. Thomson,[1] Regula Burkhard,[10] Haozhe Wang,[6] Antoine Dufour,[1,11] Markus B. Geuking,[10] Braedon McDonald,[12] Tatiana V. Petrova,[4,13] Nicola L. Harris,[2,6,15,*] and Kathy D. McCoy[1,15,16,*]

[1]Department of Physiology and Pharmacology, Snyder Institute for Chronic Diseases, University of Calgary, Cumming School of Medicine, 3330 Hospital Drive NW, Calgary, AB T2N 4N1, Canada
[2]Global Health Institute, Swiss Federal Institute of Technology, Lausanne, 1015 Lausanne, Switzerland
[3]The Francis Crick Institute, 1 Midland Road, London NW1 1AT, UK
[4]Department of Oncology, Ludwig Institute for Cancer Research Lausanne, University of Lausanne (UNIL), Chemin des Boveresses 155, Epalinges, Switzerland
[5]Maurice Müller Laboratories, Department of Biomedical Research, Universitätsklinik für Viszerale Chirurgie und Medizin Inselspital, University of Bern, Murtenstrasse 35, 3008 Bern, Switzerland
[6]Department of Immunology and Pathology, Central Clinical School, Monash University, The Alfred Centre, Melbourne, VIC, Australia
[7]Proteomics Core Facility, Federal Institute of Technology, Lausanne, 1015 Lausanne, Switzerland
[8]Monash Bioinformatics Platform, Monash University, Clayton, VIC 3168, Australia
[9]International Microbiome Centre, Cumming School of Medicine, University of Calgary, Calgary, AB, Canada
[10]Department of Microbiology, Immunology and Infectious Diseases, Snyder Institute of Chronic Diseases, Cumming School of Medicine, University of Calgary, Calgary, AB, Canada
[11]McCaig Institute for Bone and Joint Health, University of Calgary, Calgary, AB T2N 4N1, Canada
[12]Department of Critical Care Medicine, Cumming School of Medicine, University of Calgary, Calgary, AB T2N 4A1, Canada
[13]Swiss Institute for Experimental Cancer Research, School of Life Sciences, Swiss Federal Institute of Technology Lausanne, Route Cantonale, 1015 Lausanne, Switzerland
[14]These authors contributed equally
[15]Senior author
[16]Lead contact
*Correspondence: nicola.harris@monash.edu (N.L.H.), kathy.mccoy@ucalgary.ca (K.D.M.)
https://doi.org/10.1016/j.immuni.2022.05.014

## SUMMARY

The intestine harbors a large population of resident eosinophils, yet the function of intestinal eosinophils has not been explored. Flow cytometry and whole-mount imaging identified eosinophils residing in the lamina propria along the length of the intestine prior to postnatal microbial colonization. Microscopy, transcriptomic analysis, and mass spectrometry of intestinal tissue revealed villus blunting, altered extracellular matrix, decreased epithelial cell turnover, increased gastrointestinal motility, and decreased lipid absorption in eosinophil-deficient mice. Mechanistically, intestinal epithelial cells released IL-33 in a microbiota-dependent manner, which led to eosinophil activation. The colonization of germ-free mice demonstrated that eosinophil activation in response to microbes regulated villous size alterations, macrophage maturation, epithelial barrier integrity, and intestinal transit. Collectively, our findings demonstrate a critical role for eosinophils in facilitating the mutualistic interactions between the host and microbiota and provide a rationale for the functional significance of their early life recruitment in the small intestine.

## INTRODUCTION

Eosinophils are multi-functional granulocytes commonly identified as effector cells mobilized during type II immune responses. Early studies on eosinophils have largely focused on their response to helminth infection or contribution to pathophysiological processes during allergic disorders, including asthma and eosinophilic esophagitis (Huang and Appleton, 2016; Rothenberg and Hogan, 2006). In contrast, the relevance of eosinophil residence in tissues under homeostatic conditions remains elusive (Shah et al., 2020; Weller and Spencer, 2017). Accumulating evidence supports a role for eosinophils in promoting organogenesis/morphogenesis in the developing mammary gland and lung (Gouon-Evans et al., 2000; Loffredo et al., 2020), aiding the repair of injured muscle (Heredia et al., 2013) and liver (Goh et al., 2013), shedding of the uterine lining (Vicetti Miguel et al., 2017), modulating the tumor environment (Grisaru-Tal et al., 2020), and contributing

Please cite this article in press as: Ignacio et al., Small intestinal resident eosinophils maintain gut homeostasis following microbial colonization, Immunity (2022), https://doi.org/10.1016/j.immuni.2022.05.014



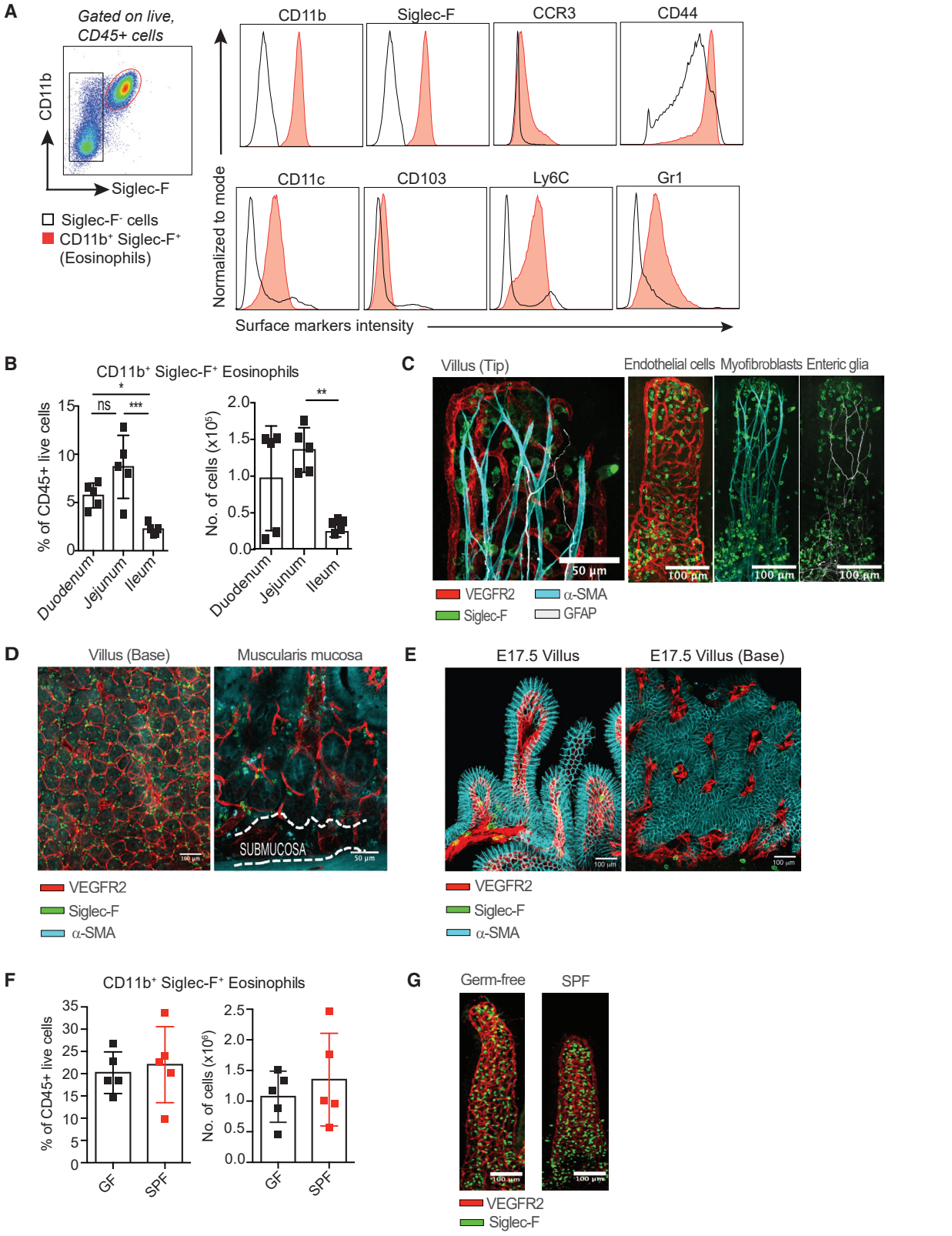


**Figure 1. SI eosinophils are localized in the villous lamina propria and recruited in a microbiota-independent manner**

(A and B) Flow cytometry analysis of eosinophils isolated from the SI lamina propria showing (A) gating strategy, mean fluorescence intensity (MFI) of surface markers, and (B) frequency of eosinophils within total CD45⁺ cells plus absolute eosinophil numbers within distinct SI regions.

*(legend continued on next page)*

Please cite this article in press as: Ignacio et al., Small intestinal resident eosinophils maintain gut homeostasis following microbial colonization, Immunity (2022), https://doi.org/10.1016/j.immuni.2022.05.014





to metabolic homeostasis in lean adipose (Qiu et al., 2014; Wu et al., 2011).

The largest population of eosinophils resides in the gastrointestinal (GI) tract. They are recruited to the gut during late gestation and early life independent of the microbiota (Jiménez-Saiz et al., 2020; Mishra et al., 1999). Gut-resident eosinophils are involved in the immunoregulation and maintenance of other immune cell populations, particularly in the small intestine (SI), both during homeostasis (Chu et al., 2014b; Jung et al., 2015; Sugawara et al., 2016) and upon bacterial infection (Arnold et al., 2018; Buonomo et al., 2016). Evidence that SI-resident eosinophils exhibit specific characteristics, such as prolonged survival (Carlens et al., 2009), altered-surface marker expression (Chu et al., 2014a), and signs of degranulation (Kato et al., 1998), suggests that these cells are regulated by the local tissue microenvironment. However, the factors that regulate their residency or activation within the SI have not been defined nor is it known whether eosinophils impact the normal physiological function of the SI.

We report an important functional consequence of eosinophil residency in the SI and demonstrate that eosinophils play a critical role in maintaining tissue homeostasis by regulating the extent of microbiota-induced alterations in the SI. We identified the microbiota as a key regulator of SI eosinophil activation, heterogeneity, and function and showed that eosinophil deficiency led to maladaptive changes in small intestinal architecture and physiology upon microbial colonization, characterized by significant villous blunting, barrier leakage, and altered peristalsis.

## RESULTS

### During homeostasis, eosinophils are enriched in the upper SI and recruited in a microbiome-independent manner

To understand the homeostatic contributions of eosinophil residency in the SI, we characterized their distribution along the SI by flow cytometry. In accordance with previous studies, eosinophils could be identified as $SSC^{high}CD45^{+}Siglec\text{-}F^{+}$ (Carlens et al., 2009; Chu et al., 2014a) with high surface expression of CD11b and Siglec-F and intermediate levels of CCR3, CD44, CD103, CD11c, Ly6C, and Gr1 (Figure 1A). Corroborating previous reports (Chu et al., 2014a), eosinophils were enriched in the duodenum and jejunum in comparison with the ileum (Figure 1B). To assess the functions of resident eosinophils, we analyzed their localization within the SI villi using whole-mount immunostaining (Bernier-Latmani and Petrova, 2016). Eosinophils were found throughout the SI lamina propria (LP) and in close proximity to stromal cells, such as α-smooth actin $(\alpha\text{-SMA})^{+}$ myofibroblasts (Figures 1C and S1A), glial cells (Figure 1C), and neural processes, including neuronal axons (Figure S1B). Eosinophils were distributed homogenously throughout the villus and crypt zones but were absent in the muscularis mucosa (Figures 1D and S1C).

Next, we analyzed eosinophil recruitment to the SI and found that eosinophils were recruited as early as embryonic day 17.5 (Figure 1E). Germ-free (GF) and colonized specific-pathogen-free (SPF) BALB/c mice harbored similar eosinophil frequencies and numbers (Figures 1F, 1G, and S1D), confirming that their initial seeding into the SI was independent of the microbiota (Mishra et al., 1999). Furthermore, eosinophil distribution within villi was not influenced by colonization status at steady state (Figure S1E). These data characterize eosinophil localization within the villous LP and corroborate earlier findings of their microbiota-independent recruitment to the SI.

### Absence of resident SI eosinophils leads to villous abnormalities and alterations in the transcriptome

To further assess the potential contributions and importance of eosinophil residency in the SI, we analyzed the impact of eosinophil deficiency using the widely employed ΔdblGATA1 mouse strain, which has complete ablation of the eosinophil lineage (Yu et al., 2002). Whole-mount imaging revealed that the absence of eosinophils impacted villous architecture characterized by a reduction in villous surface area, most pronounced in the proximal SI where eosinophils are most abundant (Figure 2A). The decreased villous area was not observed at day 7 of postnatal life, despite the absence of eosinophils, but was apparent by day 10 (Figure 2B), suggesting that it is influenced by environmental factors after birth. We also observed that NOD.SCID × $\gamma c^{-/-}$ mice, which are deficient in T, B, and NK cells (Ito et al., 2002) have diminished SI eosinophils (Figure S2A; Carlens et al., 2009) and exhibit a similar altered villous phenotype (Figure S2B). These villous defects were not simply due to reduced cellularity resulting from eosinophil loss as *Rag2*$^{-/-}$ mice, which have drastically reduced immune cellularity due to loss of T and B cells, did not exhibit villous defects (Figure S2C). To confirm that villous alterations were eosinophil specific and not due to an unappreciated impact of the ΔdblGATA1 mutation in non-hematopoietic cells, we generated bone-marrow chimeras in which ΔdblGATA1 bone marrow was transferred into irradiated BALB/c recipients. These data confirmed that ΔdblGATA1 mutation within the hemopoietic compartment was responsible for the observed villous phenotype (Figure S2D). Despite alterations in villous architecture, ΔdblGATA1 mice

(C and D) Whole-mount staining of jejunum from BALB/c mice showing (C, from left to right) villous tip view with staining for eosinophils (Siglec-F, green), blood endothelial cells (VEGFR2, red), myofibroblasts (α-SMA, cyan), and glial cells (GFAP, white); (D, from left to right) muscularis mucosa and crypt view.
(E) Whole-mount imaging of basement membrane (left) and villi (right) of BALB/c mice at E17.5 showing eosinophils (Siglec-F, green), blood endothelial cells (VEGFR2, red), and epithelial cells (E-cadherin, cyan).
(F) Flow cytometry analysis of eosinophils isolated from the SI lamina propria of germ-free (GF) or specific-pathogen-free (SPF) BALB/c mice showing frequency of eosinophils within total $CD45^{+}$ cells and absolute eosinophil numbers.
(G) Whole-mount staining of jejunum from GF or SPF BALB/c mice showing villous tip view with staining for eosinophils (Siglec-F, green) and blood endothelial cells (VEGFR2, red). Flow cytometry experiments show one experiment and are representative of four independent experiments performed using GF and SPF mice from two different animal facilities. For all panels, statistical analysis was performed using a Student's t test; $p < 0.05^{*}$, $p < 0.01^{**}$, $p < 0.001^{***}$, N.S. non-significant, each bar graph representing data mean ± SD of n = 3–5 mice per experiment with individual data points representing a single mouse.
See also Figure S1.

Please cite this article in press as: Ignacio et al., Small intestinal resident eosinophils maintain gut homeostasis following microbial colonization, Immunity (2022), https://doi.org/10.1016/j.immuni.2022.05.014



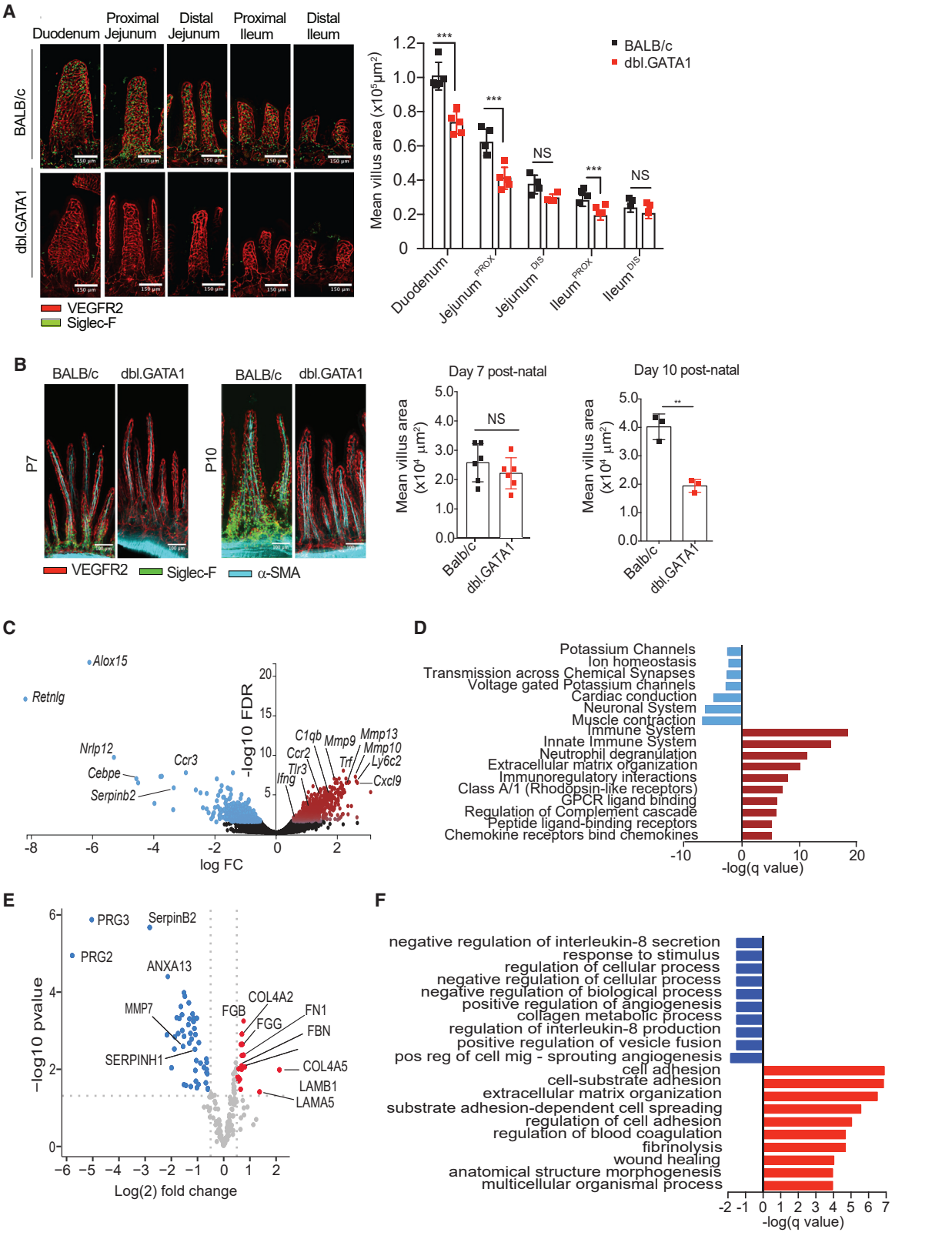


**Figure 2. Eosinophil deficiency results in villous atrophy and is associated with transcriptome alterations within the SI lamina propria**

(A) Quantification of mean villous surface area from various SI regions calculated from the vascular cage area of whole-mount tissues from adult (8–12 weeks) SPF BALB/c and ΔdbI.GATA1 mice stained for eosinophils (Siglec-F, green) and blood endothelial cells (VEGFR2, red). Images show representative villi from a single

*(legend continued on next page)*

Please cite this article in press as: Ignacio et al., Small intestinal resident eosinophils maintain gut homeostasis following microbial colonization, Immunity (2022), https://doi.org/10.1016/j.immuni.2022.05.014



exhibited similar numbers of CD45$^-$ stromal cell populations and normal proportions of the main stromal cell subsets including fibroblasts, lymphatic cells, and blood endothelial cells (Figure S2E).

To gain a broader perspective of the effects of eosinophil deficiency within the SI, we analyzed the transcriptome of intestinal epithelial cells (IECs) and LP fractions by RNA sequencing (RNA-seq). Expression of only one gene (*Cyp4a10*) was significantly altered between the entire IEC transcriptome of BALB/c and ΔdbI.GATA1 mice, suggesting that eosinophils do not influence epithelial stemness or differentiation (Figure S2F). In contrast, significant changes were observed in the transcriptome of the LP, with increased expression of 399 genes and decreased expression of 197 genes (FDR < 0.01 and $\log_2$FC > 1) in the absence of eosinophils (Table S1). As expected, transcripts reduced most strongly were those known to be associated with eosinophils, including *Alox15* (Miyata et al., 2013; Uderhardt et al., 2017), *Retnlg* (Chumakov et al., 2004; Schinke et al., 2004), *Nlrp12* (Allen et al., 2012), *Cebpe* (Gombart et al., 2003), *Ccr3* (Pope et al., 2005), and *Serpinb2* (Fulkerson et al., 2006; Swartz et al., 2004) (Figure 2C). Gene set enrichment analysis (GSEA) indicated that loss of eosinophils resulted in a positive enrichment of pathways related to innate immune/inflammatory responses, extracellular matrix (ECM) organization, G-protein-coupled receptors (GPCRs) and GPCR ligand binding, and regulation of complement cascade (Figure 2D; Table S1). We also observed a negative enrichment for pathways related to muscle contraction and neuronal signaling (Figure 2D; Table S1).

The observed enrichment of transcripts from ECM-related pathways (Figure 2D) corroborates reported associations between eosinophils and tissue remodeling in the airways (Flood-Page et al., 2003; Humbles et al., 2004). We thus investigated the impact of eosinophil deficiency on ECM composition in more depth by conducting quantitative liquid chromatography and tandem mass spectrometry (LC-MS/MS) analysis of the ECM-enriched fraction of control BALB/c or ΔdbI.GATA1 mice, using tissue obtained from the proximal jejunum where the villous phenotype was most pronounced. We observed significant changes in multiple ECM and ECM-related proteins, with 15 proteins increased and 42 proteins decreased (FDR < 0.05 and $\log_2$FC > 0.5) in samples from ΔdbI.GATA1 SI (Figure 2E; Table S2). The most reduced proteins in ΔdbI.GATA1mice included SerpinB2 and the Eosinophil Major Basic proteins (PRG2 and PRG3) (Figure 2E). Eosinophil deficiency decreased levels of matrix metalloproteinase (MMP)-7, concomitant with increased amounts of Fibronectin and multiple subunits for the basement membrane proteins Collagen alpha-4(IV) and Laminin, which are all substrates for MMP7 (Figure 2E; McGuire et al., 2003). GSEA analyses of the proteomic data indicated pathways associated with cell and cell-substrate adhesion and the tissue damage response (coagulation, fibrinolysis) (Barker and Engler, 2017; Hubbard et al., 2014; Sottile and Hocking, 2002) were enhanced in ΔdbI.GATA1 SI (Figure 2F; Table S2). Furthermore, eosinophil deficiency decreased the abundance of proteins involved in multiple pathways, including those related to angiogenesis and IL-8 (Figure 2F; Table S2). Taken together, these data indicate that the absence of eosinophils is associated with an altered transcriptome and proteome of SI connective tissue (LP minus IEC) in adulthood.

## Eosinophils contribute to intestinal homeostasis in an IL-33-dependent manner

Given the alterations to tissue architecture and the negative impact of eosinophil deficiency on angiogenic pathways, we assessed a possible role for eosinophils in regulating the villous vasculature. Density and branching analysis of the blood vessels revealed no obvious defects with regards to vessel patterning (Figure S3A). Many of the ECM proteins increased in the absence of eosinophils constituted specific components of the basement membrane that influences IEC function (Groulx et al., 2011; Vllasaliu et al., 2014) and forms an anatomical barrier between the epithelium and underlying connective tissue. Thus, we investigated the impact of eosinophil deficiency on IEC homeostasis and barrier function. In agreement with our finding in Figure S2F, IEC differentiation into Goblet cells, Tuft cells, or Paneth cells was not altered between BALB/c and ΔdbI.GATA1 mice (Figures S3B–S3D). IEC proliferation was also not affected by the absence of eosinophils (Figure 3A). Given the observed alterations of the ECM in eosinophil-deficient mice, with an enrichment of basement membrane proteins, we examined whether the migration of IEC along this membrane was altered. We observed a moderate, but consistent, delay in IEC migration in ΔdbI.GATA1 mice, as determined by tracking the distance traveled by EdU$^+$ IECs from villus-crypt axis at 24 h post-EdU labeling (Figure 3B). Delayed IEC migration was confirmed in bone marrow transfer experiments where transfer of ΔdbI.GATA1 bone marrow to irradiated BALB/c recipients recapitulated the delay in IEC migration (Figure 3C).

mouse. The bar graph shows data from one experiment and are representative of at least 2 independent experiments performed using SPF mice from two different animal facilities. Statistical analysis was performed using a multiple t test with statistical significance determined using the Holm-Sidak method; $p < 0.05$*, $p < 0.01$**, $p < 0.001$***, N.S. non-significant, each bar graph represents data mean ± SD of n = 5 mice per experiment with individual data points representing the mean surface area of at least >30 villi randomly sampled within the indicated area of tissue per mouse.

(B) Whole-mount imaging of jejunum from BALB/c and ΔdbI.GATA1 mice (littermates) at day 7 (left) and 10 postnatal (right) showing eosinophils (Siglec-F, green), blood endothelial cells (VEGFR2, red), and myofibroblasts (α-SMA, cyan). For quantification of villous area, VEGFR2 staining was used to determine villous boundary. Field or area containing at least 3 villi and 10 images were collected per mouse. Data pooled from 2–3 breeding. Statistical analysis (unpaired) Student's test **$p < 0.01$. Error bars represent SD.

(C and D) Bulk tissue RNA-seq of proximal jejunum, devoid of epithelial cells (non-IEC fraction), from BALB/c and ΔdbI.GATA1 SPF mice: (C) volcano plot showing all differentially expressed genes (DEGs) identified; (D) gene set enrichment analysis (GSEA) of gene pathways decreased (blue) or increased (red) in ΔdbI.GATA1 mice (FDR < 0.01, $\log_2$FC > 1). Only pathways with an interaction score of >0.7 are shown.

(E and F) Liquid chromatography and tandem mass spectrometry (LC-MS/MS) on extracellular matrix (ECM) enriched proteins from the proximal jejunum of BALB/c and ΔdbI.GATA1 SPF mice: (E) volcano plot showing all proteins ECM and ECM-related proteins; (F) GSEA analyses of proteomic data showing pathways decreased (blue) or increased (red) in ΔdbI.GATA1 mice (FDR < 0.05 and $\log_2$FC > 1) proteins in dbI.GATA1 mice.

See also Figure S2.

Please cite this article in press as: Ignacio et al., Small intestinal resident eosinophils maintain gut homeostasis following microbial colonization, Immunity (2022), https://doi.org/10.1016/j.immuni.2022.05.014



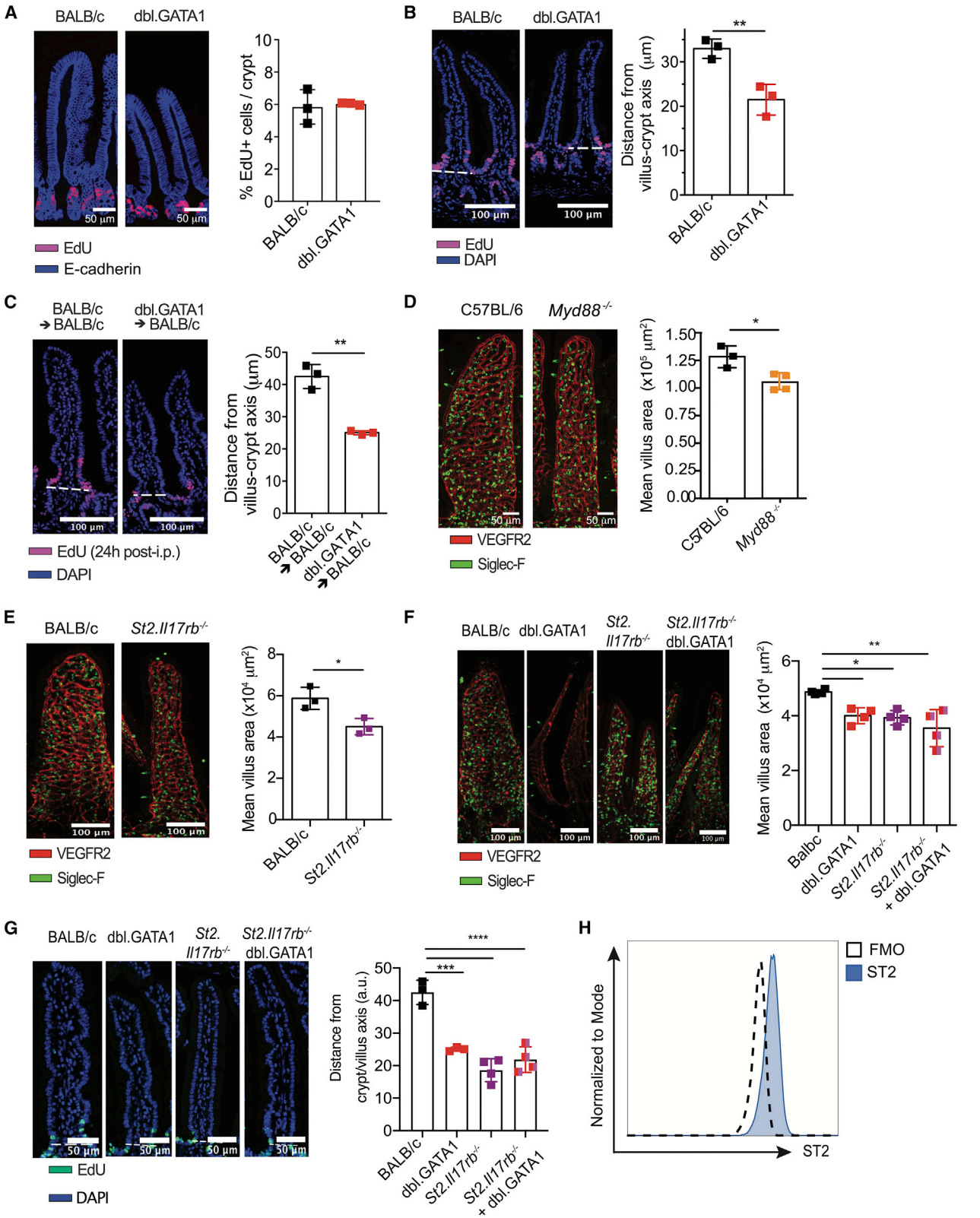


*(legend on next page)*

Please cite this article in press as: Ignacio et al., Small intestinal resident eosinophils maintain gut homeostasis following microbial colonization, Immunity (2022), https://doi.org/10.1016/j.immuni.2022.05.014





To further examine the underlying mechanisms by which eosinophils regulate villous size and IEC migration, we analyzed *Myd88*$^{-/-}$ mice, which lack microbial sensing (Kawai et al., 1999) and signaling via IL-1 receptors (IL-1Rs) (Adachi et al., 1998). *Myd88*$^{-/-}$ mice exhibited a similar villous defect to ΔdbI.GATA1 mice (Figure 3D). Given that the receptor for IL-33, IL1RL1 (ST2), requires MyD88 for signaling (Pinto et al., 2018) and emerging evidence that IL-33 can regulate eosinophil function (Angulo et al., 2019; Cherry et al., 2008; Johnston and Bryce, 2017; Suzukawa et al., 2008; Westermann et al., 2022), we analyzed villous structure in *St2/Il17rb*-deficient mice, the only ST2-deficient mice available to us on a BALB/c background. Similar to ΔdbI.GATA1 and *Myd88*$^{-/-}$ mice, *St2/Il17rb*-deficient mice also showed reduced villous size at steady state (Figure 3E). To determine whether this phenotype was due to IL-33 signaling in eosinophils or via another cell type, we generated bone-marrow chimeras in which all hematopoietic cells lacked ST2 (ST2/IL17RB) or only eosinophils lacked ST2 (ST2/IL17RB + ΔdbI.GATA1) and compared these with wild-type (BALB/c) or eosinophil-deficient (ΔdbI.GATA1) chimeras. Chimeras in which all cells, or only eosinophils, lacked ST2 exhibited the same degree of villous blunting (Figure 3F) and delayed IEC migration (Figure 3G) as the eosinophil-deficient chimeras. We also confirmed that eosinophils express ST2 (Figure 3H), as previously reported, but not IL17RB (Figure S3E), suggesting that eosinophils require the expression of the IL-33R to promote SI homeostasis. We then performed RNA-seq on SI LP of *St2/Il17rb*$^{-/-}$ mice and found that many of the genes with reduced expression overlapped with those found in ΔdbI.GATA1 mice. GSEA analysis revealed an enrichment for the same pathways that were found in ΔdbI.GATA1 mice (Figure S3F). These data support a role for IL-33 signaling in eosinophils to regulate SI homeostasis.

Given the impact of eosinophils on the ECM and IEC migration, we investigated whether eosinophil deficiency affected barrier function. *Ex vivo* explants of the SI of ΔdbI.GATA1 mice exhibited a slight increase in barrier leakage (Figure 4A), although this was not sufficient to increase serum FITC levels following oral gavage of FITC-Dextran (data not shown). This small increase in barrier leakage may explain the increased inflammatory signature (Figure 2D; Table S1), associated with a predicted activation of microbial (LPS, PolyI:C) or inflammatory pathway (IFNγ, TNF, IFNα, IRF3, MyD88, and STAT1) regulators (Table S3). These findings suggest that eosinophils may reinforce villous integrity by regulating ECM turnover and timely replacement of IECs and preventing activation of inflammatory responses by intestinal microbes. This is in line with the critical role of eosinophils to protect from inflammation during infection (Arnold et al., 2018) or protect from *Clostridium difficile* infection by enhancing epithelial integrity (Buonomo et al., 2016).

In contrast to the positively enriched ECM signature in the LP RNA-seq data, negative enrichment for neuronal and muscle contraction pathways was observed in ΔdbI.GATA1 mice (Figure 2D). Given the proximity of eosinophils to neuronal/glial cells in the LP (Figures 1C and S1B) and the importance of the enteric nervous system in regulating GI motility, we evaluated whether eosinophil deficiency impacted intestinal motility. Based on the migration of Carmine Red dye (Dey et al., 2015), ΔdbI.GATA1 mice had faster total intestinal transit time (Figure 4B), which correlated with changes in muscle contractility as assessed in an organ bath (Figure S4A). A trend toward decreased contraction frequency was also observed in the uppermost part of the SI from ΔdbI.GATA1 mice ($p < 0.0566$), although the tension remained similar over time between both ΔdbI.GATA1 and BALB/c mice (Figure S4A).

Given the impact of eosinophils on villous surface area and intestinal transit, we investigated whether these differences translate to alterations in nutrient absorption in ΔdbI.GATA1 mice. We found that under steady state, no differences in total absorptive capacity (Figure 4C) and body mass/calories absorbed (Figure 4D) were observed between BALB/c and ΔdbI.GATA1 mice. However, when mice were challenged with a bolus of olive oil via oral gavage, serum triglycerides were decreased in

**Figure 3. Signaling through MyD88 and ST2 regulate eosinophil-induced villous size alterations**

(A) Jejunum from BALB/c and ΔdbI.GATA1 SPF mice harvested 1h after EdU (200 μg/mouse) intraperitoneal injection. EdU$^{+}$ cells (purple) are showed as percentage of intestinal epithelial cells per crypt (nuclei stained with DAPI—blue). Cells were randomly sampled from >30 villi per mouse and images show representative villi from a single mouse.

(B and C) Jejunal tissues were collected 24 h after intraperitoneal injection of EdU (200 μg/mouse) injection. (B) Epithelial cell migration was assessed by measuring the distance of EdU$^{+}$ cells migrated above the villus-crypt axis (indicated by dotted-line; EdU$^{+}$ cells [purple], nuclei stained with DAPI [blue]). Panels show tissues from (B) BALB/c and ΔdbI.GATA1 SPF mice, and (C) irradiated BALB/c recipients 8 weeks after bone marrow transfer of either BALB/c or ΔdbI.GATA1. For (A)–(C), each bar represents data mean ± SD of n = 3 mice with individual data points the mean of (A) at least 75 crypts and (B and C) surface area of at least >30 villi randomly sampled within the jejunum tissue per mouse.

(D) Quantification of mean villous surface area from various SI regions calculated from the vascular cage of whole-mount tissues from SPF C57BL/6 mice versus *Myd88*$^{-/-}$ mice stained for eosinophils (Siglec-F, green) and blood endothelial cells (VEGFR2, red). Images show representative villi from a single mouse. Each bar graph represents data mean ± SD of n = 3–4 mice with individual data points representing the mean surface area of at least >30 randomly sampled villi per mouse obtained from the proximal jejunum.

(E) Quantification of mean villous surface area of jejunum from SPF BALB/c and *St2Il17rb*$^{-/-}$ mice showing villous staining for eosinophils (Siglec-F, green) and blood endothelial cells (VEGFR2, red). Images show representative villi from a single mouse. Each bar graph represents data mean ± SD of n = 3 mice with individual data points representing the mean surface area of at least >30 randomly sampled villi per mouse obtained from the proximal jejunum.

(F) Quantification of mean villus surface area from jejunum from irradiated BALB/c mice reconstituted with either bone marrow from BALB/c, ΔdbI.GATA1, or *St2Il17rb*$^{-/-}$ and chimeric marrow from *St2Il17rb*:dbI.GATA1 mixed (1:3 ratio). Each data point is an average of surface area from >30 villi randomly sampled per mouse.

(G) Same mice used in (F) were intraperitoneally injected with EdU$^{+}$ (200 μg/mouse) 24 h before harvest. Each data point is an average measurement of distance migrated by EdU$^{+}$ cells from the villus-crypt axis (dashed line). Cells were randomly sampled from >30 villi per mouse.

(H) Expression of ST2 evaluated by mean fluorescence intensity (MFI) in eosinophils (live, SSC$^{hi}$, CD45$^{+}$ Siglec-F$^{+}$) from jejunum from BALB/c mice (blue line). Fluorescence minus one (FMO) was used as control (dashed line). For all panels, statistical analysis was performed using a Student's t test $p < 0.05$*, $p < 0.01$**, $p < 0.001$***, N.S. non-significant.

See also Figure S3.

Please cite this article in press as: Ignacio et al., Small intestinal resident eosinophils maintain gut homeostasis following microbial colonization, Immunity (2022), https://doi.org/10.1016/j.immuni.2022.05.014



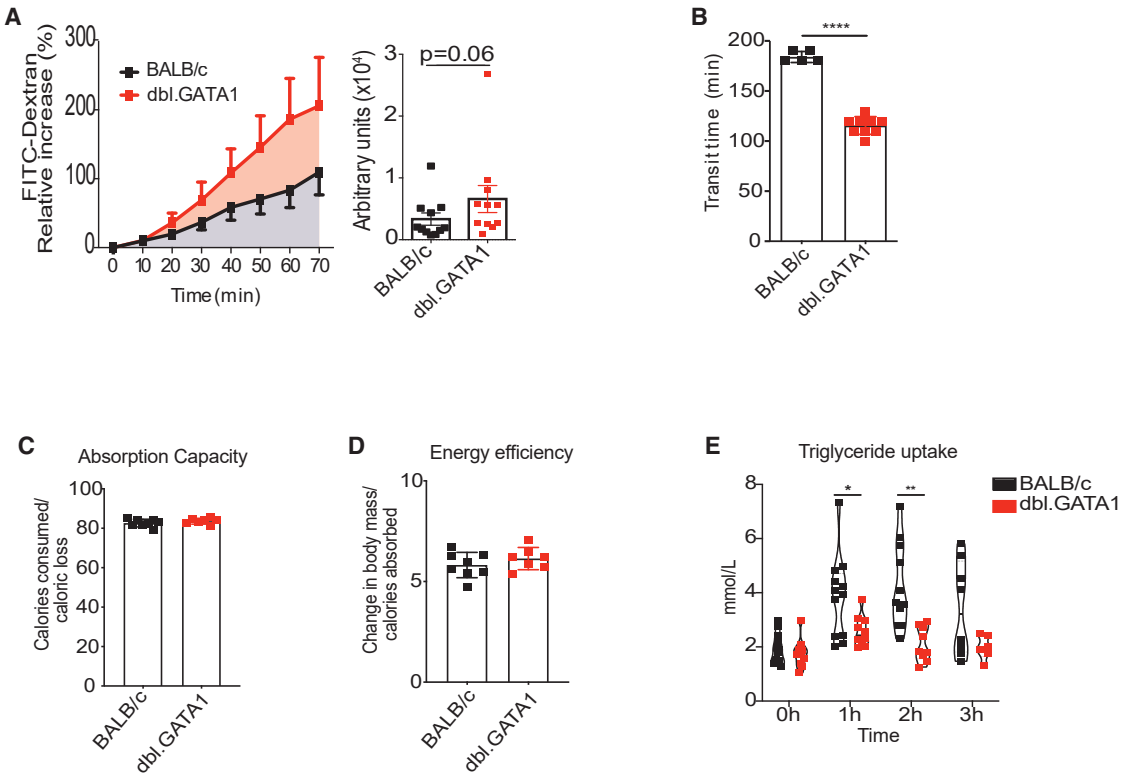


**Figure 4. Eosinophil-deficient mice exhibit alterations to barrier integrity, GI motility, and lipid absorption**

(A) Barrier integrity was analyzed using proximal jejunum fractions (2 cm) from SPF BALB/c and ΔdblGATA1 mice, with paracellular permeability to FITC-Dextran (4 kDa) evaluated every 10 min for 70 min using an Ussing Chamber. Bar graph shows area under the curve.

(B) Total intestinal transit time in SPF BALB/c and ΔdblGATA1 mice was assessed by oral gavage of Carmine Red (180 mg/mL) followed by fecal pellet harvesting. Barrier integrity and transit time plots are pooled from 2 to 3 independent experiments (n = 5–11) with individual data points each representing a single mouse. Error bars indicate SD.

(C and D) Total caloric absorption. (C) Absorption capacity (total caloric intake minus calories in feces [g]) from BALB/c and ΔdblGATA1 mice over a period of 24 h after acclimatization. (D) Energy efficiency change in body mass from beginning to end of analysis/gross caloric intake. For measurement of calories lost in feces, pellets generated over a 24 h period were collected, desiccated, and burned in a bomb calorimeter to assess energy content. Error bars represent SD within group.

(E) Triglyceride concentrations in serum of BALB/c and ΔdblGATA1 mice challenged with olive oil bolus (oral gavage) after 3 h fasting period. Data points corresponds to plasma concentrations at different time points post-gavage. Data representative of at least 2 independent experiments (n = 4–5 per group). Statistical analysis Student's t test $p < 0.05$*, $p < 0.01$**, $p < 0.001$***. Error bars represent SD within group.

See also Figure S4.

ΔdblGATA1 mice as early as 1 h after gavage (Figure 4E). Supporting altered lipid handling, ΔdblGATA1 mice showed reduced weight gain (Figure S4B) and less accumulation of fat mass (Figure S4C) compared with BALB/c littermates following 9 weeks of feeding with a high fat diet. This is in line with previous reports showing impaired fat accumulation in the absence of eosinophils (Lee et al., 2018).

Collectively, these results indicate that tissue-resident eosinophils influence various aspects of SI physiology during homeostasis, including villous architecture, barrier maintenance, intestinal motility, and lipid absorption. Such observations provide insight into the functional relevance for the residence of eosinophils within the SI.

## The microbiota is a key regulator of eosinophil activation and heterogeneity in the SI

Given the recruitment and maintenance of eosinophils to the SI prior to microbiota colonization, the postnatal development of an altered villous structure, and the barrier and physiological defects that result from eosinophil loss in SPF mice, we hypothesized that eosinophils may mitigate microbiota-induced inflammation and alterations to intestinal function. This hypothesis was supported by the observation that microbial colonization of GF mice prompted IL-33 release from IEC (Figure 5A), in line with our previous observations highlighting IL-33 as central to the impact of eosinophils on intestinal integrity. To directly test the requirement for microbial activation, we investigated eosinophil responsiveness to microbial colonization using GF versus recolonized BALB/c mice. BrdU pulse chase experiments revealed that microbial colonization resulted in shorter half-life of intestinal eosinophils, consistent with increased cellular activity and reduced survival (Figure 5B). The presence of sombrero vesicles and empty vesicles in SPF eosinophils as determined by transmission electron microscopy (TEM; Figure 5C) and lower levels of intracellular eosinophil peroxidase (EPO; Figure 5D) suggest that homeostatic degranulation of SI eosinophils is driven by the intestinal microbiota.

Please cite this article in press as: Ignacio et al., Small intestinal resident eosinophils maintain gut homeostasis following microbial colonization, Immunity (2022), https://doi.org/10.1016/j.immuni.2022.05.014



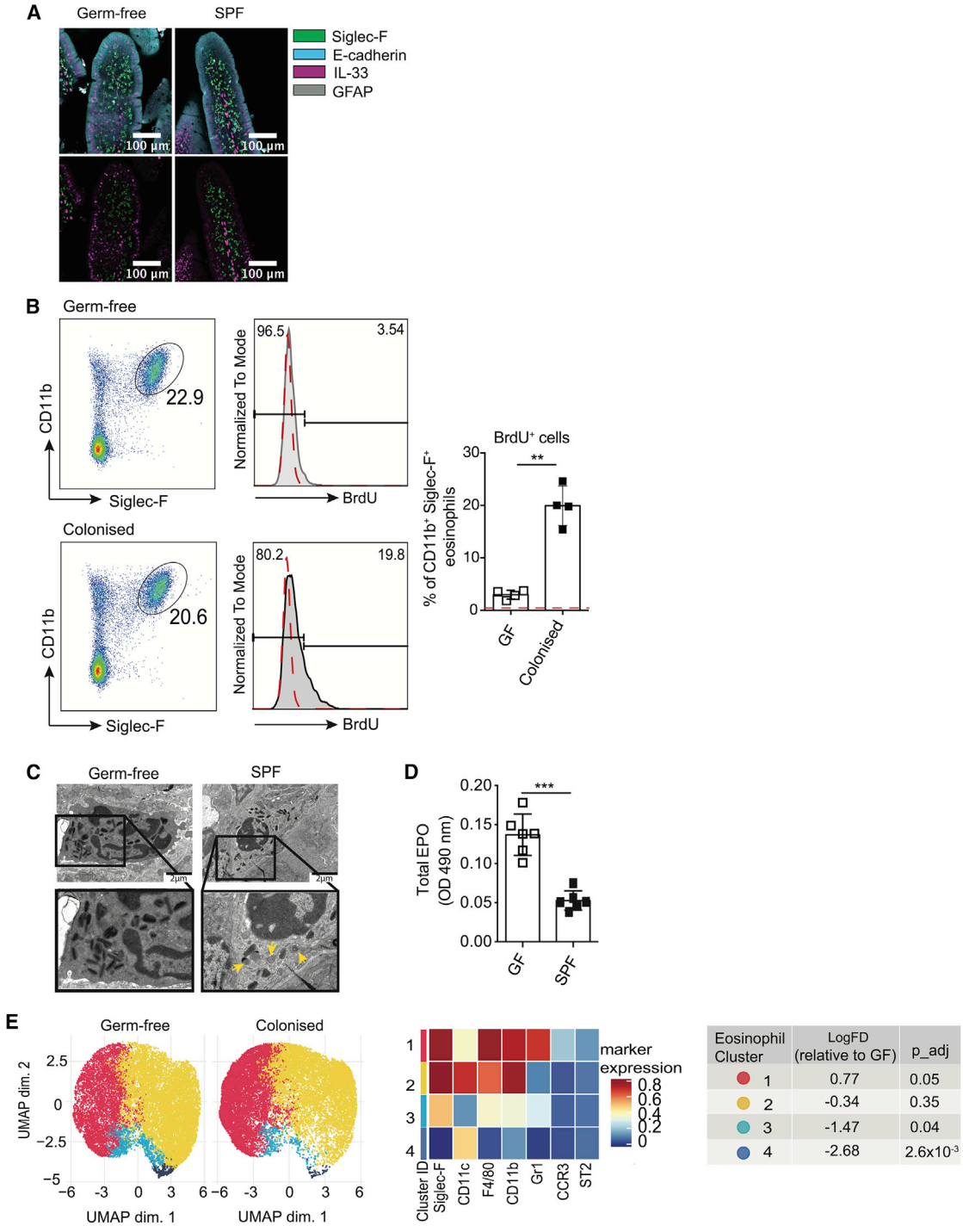


**Figure 5. The intestinal microbiota modulates the activation of SI eosinophils**

(A) Whole-mount imaging of jejunum from SPF and GF BALB/c mice showing eosinophils (Siglec-F, green), IL-33 (purple), epithelial cells (E-cadherin, blue), and glial cells (GFAP, gray).

(B) SI eosinophils were analyzed in GF and SPF BALB/c mice after all mice received BrdU in the drinking water for 8 days. Plots are representative of 2 independent experiments (n = 3–4 mice). Dotted red line indicates background fluorescence. Water consumption did not differ between groups (GF = 7.8 ± 1.8 mL/mouse/day, SPF = 8.1 ± 2.4 mL/mouse/day).

(C) Transmission electron microscopy (TEM) analysis of cytoplasmic granules of SI eosinophils from GF and SPF BALB/c mice.

(D) Total eosinophil peroxidase (EPO) activity analyzed in FACS-sorted eosinophils from the SI of GF and SPF BALB/c mice. Plots are pooled from 3 independent experiments (n = 2). Individual data points represent a pool of 8–10 mice for the acquisition of 1 × $10^5$ sorted eosinophils/well.

*(legend continued on next page)*

Please cite this article in press as: Ignacio et al., Small intestinal resident eosinophils maintain gut homeostasis following microbial colonization, Immunity (2022), https://doi.org/10.1016/j.immuni.2022.05.014



To further investigate microbial-induced eosinophil activation, we conducted cytometry by time of flight (CyTOF) analysis of SI eosinophils isolated from GF and recolonized BALB/c mice. Unsupervised analysis of the surface expression of CCR3, CD11c, Siglec-F, ST2, CD11b, F4/80, and Gr1 on eosinophils identified four clusters of eosinophils in the SI of GF and recolonized mice (Figures 5E and S5A). Microbial colonization resulted in reduced proportions of clusters 3 and 4 and increased frequency of cluster 1 (Figure 5E). Clusters 3 and 4 were characterized by lower expression of Siglec-F, F4/80, CD11b, Gr-1, and CCR3 (Figures 5E and S5B), suggesting these are immature eosinophils. Cluster 1 was characterized by high expression of Siglec-F, F4/80, CD11b, and Gr-1, corresponding to a mature/activated phenotype (Figures 5E and S5B). These markers are associated with eosinophil activation in response to intestinal inflammation (Arnold et al., 2018; Griseri et al., 2015), indicating that microbial colonization regulates the activation and/or maturation of intestinal eosinophils. Single-cell RNA-seq of murine eosinophils also indicated that eosinophil maturation in the gut is driven by microbiota-derived signals (Gurtner et al., 2021). Taken together, our results show that eosinophils respond to microbial colonization and play a critical role in facilitating homeostatic host-microbiota crosstalk by maintaining barrier integrity and regulating microbiota-dependent changes in intestinal physiology.

## Microbial colonization drives homeostatic SI eosinophil function

To address whether the loss of homeostasis in the absence of eosinophils was driven by the microbiota, we re-derived ΔdbI.GATA1 mice to GF status. ΔdbI.GATA1 and control BALB/c mice exhibited similar villous surface areas when reared under GF conditions (Figure 6A). In contrast, microbial colonization resulted in marked villous atrophy in both ΔdbI.GATA1 and BALB/c mice, but the presence of eosinophils in BALB/c mice mitigated the extent of the induced atrophy (Figure 6A). This was not due to altered microbial composition between ΔdbI.GATA1 and BALB/c mice. No changes in bacterial family members were observed in cecum contents of littermates 4 weeks after colonization (Figure 6B) or luminal contents from cecum, colon, and SI or colonic mucus-associated bacteria in ΔdbI.GATA1 and BALB/c mice that were co-housed or housed separately for 15 weeks of colonization with littermate SPF colonizer mice (Figure S6A). In the absence of microbial differences, we also did not observe any differences in intestinal immunoglobulin (Ig) A levels at 15 weeks post-colonization (Figure S6B), in keeping with other studies showing that IgA did not differ between wild-type and eosinophil-deficient littermates (Beller et al., 2020; FitzPatrick et al., 2020).

Intestinal macrophages are key innate cells that regulate immunity and host defense. Although a small proportion of intestinal macrophages are derived from the fetal liver and maintained through self-renewal (Shaw et al., 2018), the majority are continuously seeded from bone-marrow-derived monocytes and then differentiate locally (Bain et al., 2014), in a process that is dependent on the microbiota (Kang et al., 2020). We found that under GF conditions, the total number of $CD64^{+}CD11b^{+}$ monocyte/macrophage in the SI did not differ between BALB/c and ΔdbI.GATA1 mice (Figures S6C and S6D). In contrast, the microbial-induced increase in total monocyte/macrophage numbers observed in BALB/c mice was blunted in ΔdbI.GATA1 mice (Figure S6E). A more detailed analysis revealed that although the number of newly recruited bone-marrow-derived $Ly6C^{+}MHCII^{-}$ monocytes and differentiating immature $Ly6C^{+}MHCII^{+}$ did not differ, the number of mature $Ly6C^{-}MHCII^{+}$ macrophages within the SI LP was reduced in ΔdbI.GATA1 mice following colonization (Figures 6C–6E). This suggests that SI eosinophils promote the maturation or survival of mature intestinal macrophages following microbial colonization. Mature intestinal macrophages regulate the intestinal barrier (Chiaranunt et al., 2021; Muller et al., 2014). In line with this, we observed that although GF ΔdbI.GATA1 and BALB/c mice did not exhibit differences in permeability or intestinal transit time (Figures 6F and 6G), microbial colonization resulted in increased permeability and transit time in the absence of eosinophils (Figures 6F and 6G).

We next utilized a more sensitive measure of barrier integrity, whereby the induction of systemic bacteria-specific IgG was used to detect translocation of luminal bacteria (Zeng et al., 2016). To validate a role for eosinophils in regulating barrier integrity *in vivo*, we monocolonized GF ΔdbI.GATA1 and BALB/c mice with *Akkermansia muciniphila*, a known inducer of IgG-class switching (Ansaldo et al., 2019), and determined *A. muciniphila*-specific IgG levels in the serum using bacterial flow cytometry. In support of the observed increase in intestinal permeability following complex microbial colonization (Figure 6F), monocolonized ΔdbI.GATA1 mice displayed increased *A. muciniphila*-specific IgG2a, IgG2b, and IgG3 in serum compared with monocolonized BALB/c mice (Figure S6F). We then assessed whether the ECM-alterations observed in SPF ΔdbI.GATA1 mice (Figure 2E) were also driven in response to the microbiota. Proteome analysis of whole jejunum tissue segments from GF and recolonized ΔdbI.GATA1 and BALB/c mice revealed no significant changes in ECM or ECM affiliated proteins between GF ΔdbI.GATA1 and BALB/c mice (Table S4). In contrast, and in line with our findings in SPF mice, recolonization of GF ΔdbI.GATA1 and BALB/c mice led to increases in a number of ECM proteins, including laminins and tight/adherens junction-related proteins, which was exacerbated in the absence of eosinophils (Figure S6G; Table S5). These data suggest that alterations in the ECM in the absence of eosinophils are driven in response to the microbiota. Collectively, these observations indicate that eosinophils respond to microbial colonization, and this response is required to promote SI tissue homeostasis.

(E) CyTOF analysis of eosinophils from the proximal jejunum of GF and SPF BALB/c mice (n = 3–4). Cells were manually pre-gated on singlets (191IrDNA-event length), live (195Pt cisplatin−), 89Y $CD45^{+}$ cells on FlowJo and individual FSC files were concatenated for each group and exported for analysis by unsupervised method. Proximal jejunum eosinophils were identified and clustered using uniform manifold approximation and projection (UMAP) algorithm. Heatmap of surface marker expression considered for eosinophil identification and cluster analyses showed in the UMAP representation. Eosinophils numbers on each cluster were determined and significant differences within clusters are represented as fold change relative to GF.
See also Figure S5.

Please cite this article in press as: Ignacio et al., Small intestinal resident eosinophils maintain gut homeostasis following microbial colonization, Immunity (2022), https://doi.org/10.1016/j.immuni.2022.05.014





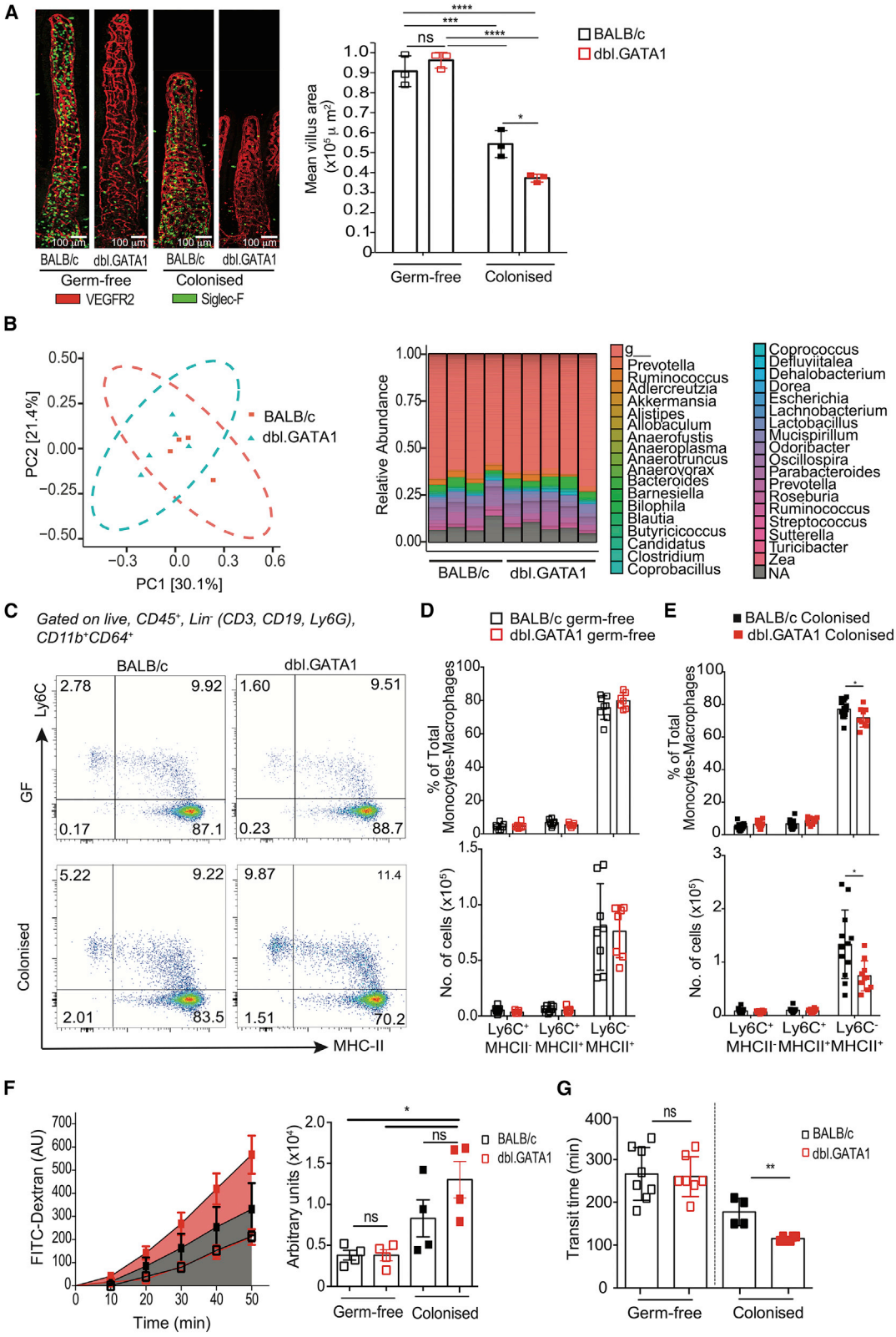


(legend on next page)

Please cite this article in press as: Ignacio et al., Small intestinal resident eosinophils maintain gut homeostasis following microbial colonization, Immunity (2022), https://doi.org/10.1016/j.immuni.2022.05.014



### Eosinophil transfer rescues the microbial-induced loss of intestinal homeostasis in eosinophil-deficient mice

To investigate if eosinophils were able to rescue the loss of SI homeostasis in Δdbl.GATA1 mice following microbial colonization, we performed eosinophil transfers into SPF Δdbl.GATA1 mice. Following transfer of bone-marrow-derived eosinophils generated *in vitro* (Figure S7A), increased numbers of eosinophils were detected in the SI LP (Figure S7B). Eosinophil transfer into adult Δdbl.GATA1 mice rescued villous atrophy (Figure 7A), normalized intestinal transit time (Figure 7B), and led to an increase in the number of Ly6C$^-$MHCII$^+$ mature macrophages in the SI (Figure 7C). The number of mature macrophages directly correlated with the number of eosinophils that repopulated the SI (Figure 7D). These data confirm that eosinophils in the SI directly regulate homeostasis in response to microbial colonization.

## DISCUSSION

The intestine undergoes significant morphological and physiological alterations in response to microbial colonization, with GF mice exhibiting thinner and longer villi (Smith et al., 2007), decreased permeability (Hayes et al., 2018), and reduced intestinal motility (Muller et al., 2014), when compared with mice colonized with a complex microbiota. The finding that eosinophil-deficient mice exhibit exaggerated microbial-induced villous blunting and increased intestinal permeability following microbial colonization reveals an unexpected function for these cells as crucial regulators of the host adaptation to the presence of intestinal bacteria. Luminal bacterial products are known to induce inflammation and an associated tissue remodeling response (van Tol et al., 1999), and our RNA-seq data revealed that eosinophil deficiency resulted in the upregulation of inflammatory pathways. Our observations that eosinophils modulate microbial-induced alterations to intestinal morphology and permeability, alongside the presence of a ECM signature indicative of persistent tissue remodeling in the absence of eosinophils, may well result from a role for these cells in dampening microbial-induced inflammation. Mechanistically, eosinophils may regulate intestinal integrity by directly contributing to the tissue remodeling processes, either via alterations to fibroblast function or direct interactions with the ECM. Eosinophil secretion of products that modulate ECM deposition and degradation (Shah et al., 2020), and involvement in tissue remodeling in the breast (Gouon-Evans et al., 2002; Gouon-Evans et al., 2000) and uterus (Vicetti Miguel et al., 2017) support the latter hypothesis. The increased intestinal permeability in eosinophil-deficient mice may also be linked to the delayed epithelial cell migration and associated alterations in basement membrane proteins. The basement membrane plays a crucial role in guiding the migration of newly differentiated enterocytes from the crypt to villous tip (Heath, 1996). We observed increases in ECM components that drive epithelial migration and re-epithelialization/wound closure (e.g., Collagen VI, Laminins) and a decrease in proteases known to regulate the turnover and/or structure/bundling of these components, including MMP7, Cathepsin B, and Serpin H1 (Li et al., 2016). These findings suggest that SI eosinophils may function as both positive and negative regulators of ECM deposition organization and composition. Alterations in the ECM, particularly enzymes differentially expressed either at a transcriptomic and/or proteomic level, are also noted to influence the bioavailability of growth and migratory factors, which could have effects on immunity and regenerative responses (Chester and Brown, 2017).

We provide evidence for SI eosinophils in modulating intestinal motility, which is influenced by neuroimmune interactions (Wang et al., 2022). Eosinophils were found in close contact with enteric glia and neural processes, and our transcriptomic analysis revealed alterations in pathways related to neuronal and muscular signaling, associated with alterations in the patterning of cyclic muscle contractions and increased intestinal motility. Of note, various receptors, adhesion molecules, and

**Figure 6. Eosinophils regulate microbial-induced villous size alterations, macrophage maturation, epithelial barrier integrity, and intestinal transit**

Germ-free (GF) BALB/c and eosinophil-deficient (Δdbl.GATA1) mice were compared with previously germ-free (ex-GF) BALB/c and Δdbl.GATA1 mice recolonized for 4 weeks with microbiota from specific-pathogen-free (SPF) BALB/c donors.

(A) Whole-mount tissues from the proximal jejunum were stained for eosinophils (Siglec-F, green) and blood endothelial cells (VEGFR2, red). Images show representative villi from a single mouse. Bar graphs show quantification of mean villous surface area, calculated using the vascular cage. Data from one experiment are shown and indicate mean ± SD of n = 3 mice with individual data points representing the mean surface area of at least >30 villi randomly sampled within the jejunum tissue per mouse. Data are representative of 2 independent experiments. Statistical analysis was performed using two-way ANOVA, Tukey's multiple comparisons post-test; $p < 0.05$*, $p < 0.01$***, $p < 0.0001$****, N.S. non-significant.

(B) 16S rRNA gene sequencing analysis of cecum content harvested from recolonized BALB/c and Δdbl.GATA1 mice.

(C) Representative FACS plots showing gating strategy for monocyte-macrophage populations from GF and colonized BALB/c and Δdbl.GATA1 mice.

(D and E) Bar graphs showing frequency of recently recruited monocytes (Ly6C$^+$MHCII$^-$), monocyte-macrophage intermediates (Ly6C$^+$MHCII$^+$), matured macrophages (Ly6C$^-$MHCII$^+$) within live CD45$^+$ Lin$^-$ (CD3, CD19, Ly6G) CD11b$^+$CD64$^+$ cells and absolute cell numbers in GF (D), and recolonized mice (E). Statistical analysis was performed using two-way ANOVA, Tukey's multiple comparisons post-test; $p < 0.05$*, $p < 0.01$**, $p < 0.001$***, N.S. non-significant, each bar graph represents data mean ± SD of n = 3–4 mice with individual data points representing a single mouse. Data are representative of 3 independent experiments.

(F) Barrier integrity was analyzed using proximal jejunum fractions (2 cm). Paracellular permeability to FITC-Dextran (4 kDa) was evaluated over a total period of 70 min using an Ussing Chamber. Bar graph shows area under the curve.

(G) Total transit time was assessed by oral gavage of Carmine Red (180 mg/mL) followed by fecal pellet harvesting. Barrier integrity and transit time plots are representative of 2–3 independent experiments (n = 4–8 mice) with individual data points representing a single mouse.

(F and G) Statistical analysis were performed using a two-way ANOVA, Tukey's multiple comparisons post-test; $p < 0.05$*, $p < 0.01$**, $p < 0.001$***, N.S. non-significant.

(E) Dashed line show GF and colonized separation for statistical analysis using Student's t test; $p < 0.05$*, $p < 0.01$**, $p < 0.001$***, N.S. non-significant. All experiments shown were repeated using GF recipient and SPF donor mice sourced from two different facilities.

See also Figure S6.

Please cite this article in press as: Ignacio et al., Small intestinal resident eosinophils maintain gut homeostasis following microbial colonization, Immunity (2022), https://doi.org/10.1016/j.immuni.2022.05.014



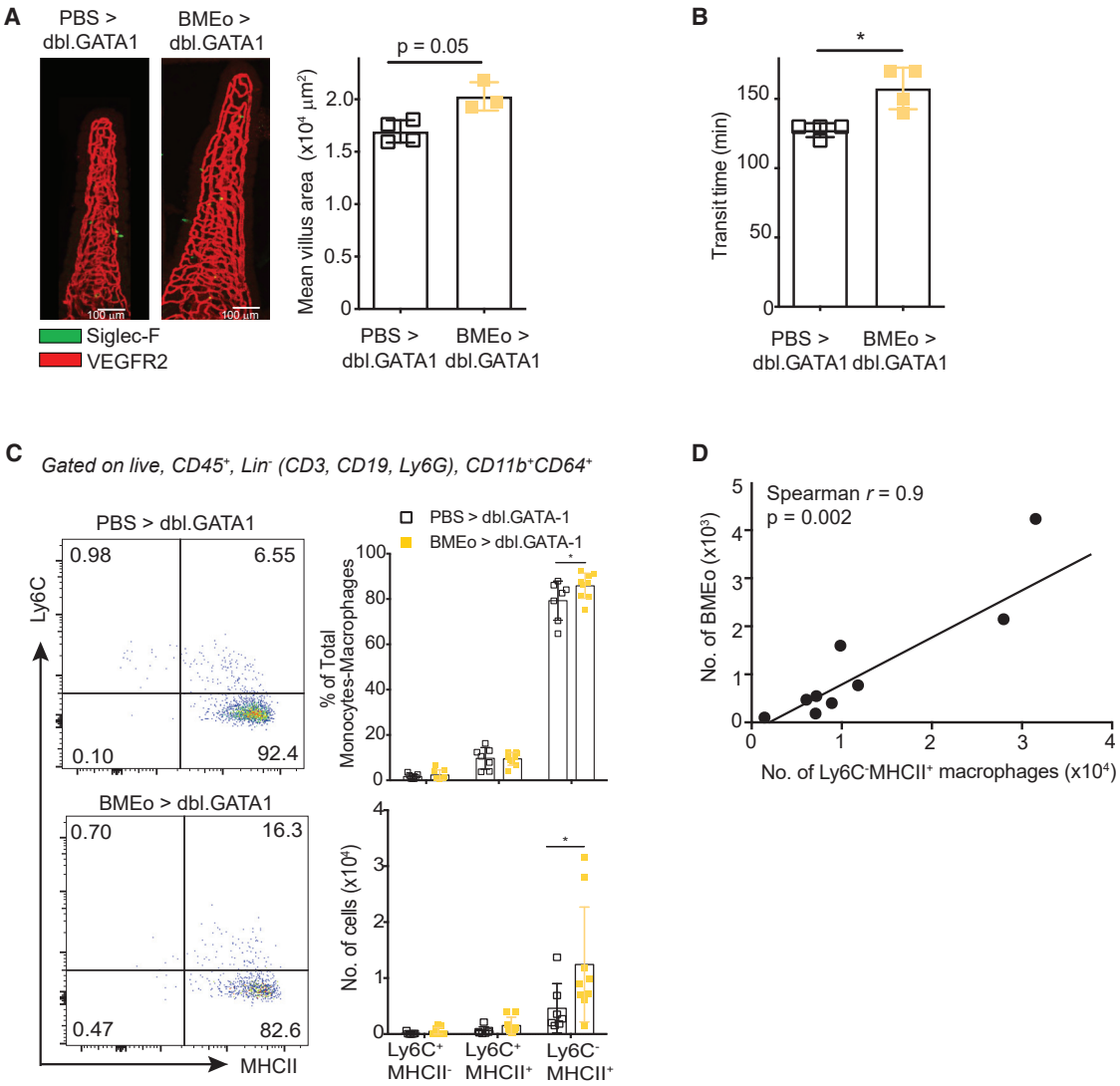


**Figure 7. Bone-marrow-derived eosinophil transfer into eosinophil-deficient mice reconstitutes villous size abnormalities, intestinal motility, and macrophage maturation in SI**

(A–D) ΔdbI.GATA1 mice were intravenously injected with PBS or BMEo.

(A) Whole-mount staining of jejunum from showing villous staining for eosinophils (Siglec-F, green) and blood endothelial cells (VEGFR2, red). For quantification of villous area, VEGFR2 staining was used to determine villous boundary.

(B) Total transit time was assessed by oral gavage of Carmine Red (180 mg/mL) followed by fecal pellet harvesting.

(A and B) Statistical analysis Student's t test $p < 0.05$*. Error bars represent SD within group.

(C) Bar graphs showing frequency of recently recruited monocytes (Ly6C$^+$MHCII$^-$), monocyte-macrophage intermediates (Ly6C$^+$MHCII$^+$), matured macrophages (Ly6C$^-$MHCII$^+$) within live CD45$^+$ Lin$^-$ (CD3, CD19, Ly6G) cells, and absolute cell numbers. Error bars represent SD within group.

(D) Correlation analysis between the number of BMEo migrated into the jejunum and number of matured macrophages (Ly6C$^-$MHCII$^+$). Statistical analysis was performed using two-way ANOVA, Tukey's multiple comparisons post-test; $p < 0.05$*, $p < 0.01$**, $p < 0.001$***.

See also Figure S7.

potassium/calcium channels involved in the regulation of neuronal action-potential/excitability were differentially expressed in ΔdbI.GATA1 mice. The precise influence of eosinophils in the regulation of intestinal motility are unclear and may reflect direct effects on muscle cells. However, given the close proximity of eosinophils to neuronal axons and reports linking eosinophils to altered neuronal growth function (Drake et al., 2018), eosinophils can likely regulate aspects of neuronal function. Indeed, intestinal bacterial and helminth pathogens can mediate protection of neurons in the gut in a process involving macrophages and eosinophils (Ahrends et al., 2021).

Microenvironmental cues specific to the intestine have been proposed to regulate eosinophil survival (Carlens et al., 2009; Mishra et al., 1999). Factors shown to be important include eotaxin (Mishra et al., 1999) and γc-dependent signals (IL-4, IL-7, IL-15, and IL-21) (Carlens et al., 2009). Our results reveal the microbiota as an additional regulator of eosinophil turnover within the SI. We show that microbiota stimulates the release of IL-33

Please cite this article in press as: Ignacio et al., Small intestinal resident eosinophils maintain gut homeostasis following microbial colonization, Immunity (2022), https://doi.org/10.1016/j.immuni.2022.05.014



from IEC, and eosinophil expression of the IL-33R was required to regulate homeostasis and prevent villous atrophy. IL-33 has been previously shown to be a potent activator of eosinophils (Johnston and Bryce, 2017).

Although the recruitment of eosinophils does not require the microbiota, microbial colonization led to increased eosinophil turnover and activation. Our data indicate that the SI contains at least 4 different clusters of eosinophils, in line with studies suggesting that eosinophils exist as a heterogeneous group of cells, whose biology and phenotype is modulated by environment cues (Abdala-Valencia et al., 2018; Shah et al., 2020). An intestinal CD11c$^{high}$ eosinophil subpopulation closely associated with the intraepithelial lymphocyte (IEL) fraction and distinct from eosinophils found in the intestinal LP and blood has been identified (Xenakis et al., 2018). In models of allergic airway inflammation, eosinophils increase Siglec-F and CD11c expression and exhibit altered morphology following their migration from the lung interstitium into the airways (Abdala Valencia et al., 2016). Lung resident eosinophils exhibiting intermediate levels of Siglec-F were found to exert regulatory functions, although inflammatory eosinophils recruited in response to allergen challenge were defined by increased Siglec-F expression and a more segmented nucleus. These cells were also able to migrate into the airways and contributed to inflammation (Mesnil et al., 2016). The intestine is unique in that it is constantly subject to a high level of remodeling and epithelial cell turnover, driven by the presence of a complex microbiota (Agace and McCoy, 2017). Thus, it is not surprising that microbial colonization leads to an increase in the eosinophil cluster defined by the highest expression levels of Siglec-F and CD11c, akin to that observed in response to inflammatory subsets within the lung. Siglec-F has been shown to promote IL-33-induced cytokine release from eosinophils (Westermann et al., 2022). Our data indicate that microbiota indirectly activates eosinophils via IEC release of IL-33; however, it is possible that other signals of tissue stress and damage (Smith et al., 2007) or direct microbial activation also takes place. Alternatively, eosinophils are noted to express pattern recognition receptors (PRRs) (Nagase et al., 2003) potentially allowing direct bacterial recognition and consequent eosinophil activation.

Intestinal macrophages maintain homeostasis and dampen inflammation in the intestine, regulate intestinal permeability, and support neuronal homeostasis (Bain and Schridde, 2018; Chiaranunt et al., 2021), and their turnover and functional diversification is known to be driven by the microbiota (Chen et al., 2022; Kang et al., 2020). Our data show that eosinophils promote the "monocyte waterfall" pathway maturation of newly recruited bone-marrow-derived monocytes within the SI environment following colonization. Eosinophils are known to produce many cytokines involved in macrophage maturation and function, including TGF-β (Chu et al., 2014b). Alternatively, eosinophils could regulate the survival of mature macrophages.

In summary, our findings demonstrate a key role for eosinophils in facilitating host adaptation to microbial colonization by regulating microbial-induced alterations to intestinal morphology and physiology. This likely involves concerted interactions with the ECM and with other key cellular nodes, including macrophages, within the villous LP. Furthermore, we reveal intestinal eosinophils to be a heterogeneous population whose phenotype is modulated by microbiota-driven signals. These signals, either directly or indirectly, regulate eosinophil activation and maturation within the intestine, thus arming these cells with the ability to modulate host tissue function. One of these signals appears to be IL-33, released in response to microbial colonization. Our findings that eosinophils impact on key structural components of the intestine, including barrier integrity, ECM organization, and motility, widen our appreciation of how these cells influence the function of healthy tissues. Our work indicates that a more holistic evaluation of tissue function is needed when assessing the mechanisms underlying eosinophil function in both health and disease. Further investigation into the mechanisms underlying microbial- or inflammation-driven activation of distinct eosinophil subsets is warranted. Understanding these mechanisms could provide insight into drivers of intestinal homeostasis versus disease and may provide novel therapeutic targets for the intervention of eosinophil-associated disorders.

### Limitations of the study

Although our study suggested that eosinophils required expression of the IL-33R to maintain homeostasis in response to microbial colonization, we utilized mice deficient in both the IL-33R and the IL-25R. Although it is unlikely that IL-25 signaling is playing a role in modulating eosinophil function due to lack of expression, further studies using ST2-deficient eosinophils will provide additional understanding of this signaling pathway. Although intestinal eosinophils have pleiotropic functions, the precise mechanisms by which eosinophils regulate tissue homeostasis remain unclear. Open questions include the following: how do eosinophils affect intestinal villus remodeling and influence intestine motility? What factors produced by eosinophils modulate macrophage differentiation? Do eosinophils also directly sense microbial-derived products or metabolites?

## STAR★METHODS

Detailed methods are provided in the online version of this paper and include the following:

- KEY RESOURCES TABLE
- RESOURCE AVAILABILITY
  - Lead contact
  - Materials availability
  - Data and code availability
- EXPERIMENTAL MODEL AND SUBJECT DETAILS
  - Mice
- METHOD DETAILS
  - Wholemount imaging
  - Histological analysis using IHC and IF
  - RNA-seq experiment
  - Chimera experiment
  - Quantitative mass spectrometry of ECM-enriched fraction
  - Quantification and statistical analysis of ECM-enriched fraction proteomic data
  - 16S analysis/16S rRNA gene amplicon sequencing
  - Intestinal contractility ex vivo
  - Lamina propria cell isolation
  - Flow cytometry and flow cytometry sorting

- Intestinal permeability (Ussing Chamber assay)
- Transit time (Carmine Red assay)
- Bacterial flow cytometry
- Immunoglobulin electrochemiluminescence immunoassay
- Shotgun Proteomics Whole Protein Dimethylation and Mass Spectrometry (MS)
- High-Performance Liquid Chromatography (HPLC) and Mass Spectrometry (MS) (Germ-free and colonised mice experiments)
- Proteomic Data and Bioinformatics Analysis (Germ-free and colonised mice experiments)
- Detection of proliferating cells with anti-BrdU
- Transmission Electron Microscopy (TEM)
- Degranulation of Eosinophil Peroxidase (EPO)
- Mass Cytometry (CyTOF) Staining and Acquisition
- CyTOF Analysis
- Bone Marrow-Derived Eosinophil (BMEo) Culture
- Bomb Calorimetry (Indirect calorimetry)
- Triglyceride Analysis
- High-fat diet experiment
- Intestinal fluid collection
- IgA ELISA

● QUANTIFICATION AND STATISTICAL ANALYSIS

## SUPPLEMENTAL INFORMATION

Supplemental information can be found online at https://doi.org/10.1016/j.immuni.2022.05.014.

## ACKNOWLEDGMENTS

We thank M. Dicay for performing Ussing Chamber experiments and S. Luther for providing *Myd88*$^{-/-}$ mice. A.I. was supported by a Fellowship from São Paulo Research Foundation (2016/15882-7) and an Eyes High Postdoctoral Fellowship from the University of Calgary. This work was supported by grants from the Swiss National Science Foundation (SNSF310030_134902 to K.D.M., SNSF310030_156517 to N.L.H., and 31003A-156266 to T.V.P.) and the European Research Council (ERC, FP/2007-2013) Agreement no. 281785 to K.D.M. K.D.M. is also supported by a Canadian Institutes of Health Research (CIHR) grant (PJT-165930). N.L.H. is supported by a National Health and Medical Research Council (NHMRC) of Australia SRF-B fellowship. A.D. was supported by an NSERC Discovery Grant (DGECR-2019-00112). The IMC is supported by the Cumming School of Medicine, University of Calgary, Western Economic Diversification (WED), and Alberta Economic Development and Trade (AEDT), Canada. Graphical Abstract was created with BioRender.com.

## AUTHOR CONTRIBUTIONS

A.I., K.S., J.B.-L., Y.K., G.C., M.M., R.H., N.C.W., C.A.T., R.B., H.W., A.D., and M.B.G. performed experiments and analyzed data. F.A. and H.R. performed bioinformatics. B.M. supervised CyTOF experiments and analysis. A.I., K.S., N.L.H., and K.D.M. wrote the manuscript, and all authors revised the manuscript and approved its final version. N.L.H. and K.D.M. conceived the project. T.V.P., N.L.H., and K.D.M. supervised the project.

## DECLARATION OF INTERESTS

The authors declare no competing interests.

Received: February 8, 2022
Revised: April 29, 2022
Accepted: May 18, 2022
Published: June 15, 2022

## REFERENCES

Abdala Valencia, H., Loffredo, L.F., Misharin, A.V., and Berdnikovs, S. (2016). Phenotypic plasticity and targeting of Siglec-F(high) CD11c(low) eosinophils to the airway in a murine model of asthma. Allergy *71*, 267–271.

Abdala-Valencia, H., Coden, M.E., Chiarella, S.E., Jacobsen, E.A., Bochner, B.S., Lee, J.J., and Berdnikovs, S. (2018). Shaping eosinophil identity in the tissue contexts of development, homeostasis, and disease. J. Leukoc. Biol. *104*, 95–108.

Adachi, O., Kawai, T., Takeda, K., Matsumoto, M., Tsutsui, H., Sakagami, M., Nakanishi, K., and Akira, S. (1998). Targeted disruption of the MyD88 gene results in loss of IL-1- and IL-18-mediated function. Immunity *9*, 143–150.

Agace, W.W., and McCoy, K.D. (2017). Regionalized development and maintenance of the intestinal adaptive immune landscape. Immunity *46*, 532–548.

Ahrends, T., Aydin, B., Matheis, F., Classon, C.H., Marchildon, F., Furtado, G.C., Lira, S.A., and Mucida, D. (2021). Enteric pathogens induce tissue tolerance and prevent neuronal loss from subsequent infections. Cell *184*, 5715–5727.e12.

Allen, I.C., Lich, J.D., Arthur, J.C., Jania, C.M., Roberts, R.A., Callaway, J.B., Tilley, S.L., and Ting, J.P. (2012). Characterization of NLRP12 during the development of allergic airway disease in mice. PLoS One *7*, e30612.

Angulo, E.L., McKernan, E.M., Fichtinger, P.S., and Mathur, S.K. (2019). Comparison of IL-33 and IL-5 family mediated activation of human eosinophils. PLoS One *14*, e0217807.

Ansaldo, E., Slayden, L.C., Ching, K.L., Koch, M.A., Wolf, N.K., Plichta, D.R., Brown, E.M., Graham, D.B., Xavier, R.J., Moon, J.J., and Barton, G.M. (2019). Akkermansia muciniphila induces intestinal adaptive immune responses during homeostasis. Science *364*, 1179–1184.

Arnold, I.C., Artola-Borán, M., Tallón de Lara, P., Kyburz, A., Taube, C., Ottemann, K., van den Broek, M., Yousefi, S., Simon, H.U., and Müller, A. (2018). Eosinophils suppress Th1 responses and restrict bacterially induced gastrointestinal inflammation. J. Exp. Med. *215*, 2055–2072.

Bain, C.C., Bravo-Blas, A., Scott, C.L., Perdiguero, E.G., Geissmann, F., Henri, S., Malissen, B., Osborne, L.C., Artis, D., and Mowat, A.M. (2014). Constant replenishment from circulating monocytes maintains the macrophage pool in the intestine of adult mice. Nat. Immunol. *15*, 929–937.

Bain, C.C., and Schridde, A. (2018). Origin, differentiation, and function of intestinal macrophages. Front. Immunol. *9*, 2733.

Baril, J.F., Bromberg, S., Moayedi, Y., Taati, B., Manlhiot, C., Ross, H.J., and Cafazzo, J. (2019). Use of free-living step count monitoring for heart failure functional classification: validation study. JMIR Cardio *3*, e12122.

Barker, T.H., and Engler, A.J. (2017). The provisional matrix: setting the stage for tissue repair outcomes. Matrix Biol. *60–61*, 1–4.

Beller, A., Kruglov, A., Durek, P., von Goetze, V., Werner, K., Heinz, G.A., Ninnemann, J., Lehmann, K., Maier, R., Hoffmann, U., et al. (2020). Specific microbiota enhances intestinal IgA levels by inducing TGF-beta in T follicular helper cells of Peyer's patches in mice. Eur. J. Immunol. *50*, 783–794.

Bernier-Latmani, J., and Petrova, T.V. (2016). High-resolution 3D analysis of mouse small-intestinal stroma. Nat. Protoc. *11*, 1617–1629.

Buonomo, E.L., Cowardin, C.A., Wilson, M.G., Saleh, M.M., Pramoonjago, P., and Petri, W.A., Jr. (2016). Microbiota-regulated IL-25 increases eosinophil number to provide protection during Clostridium difficile infection. Cell Rep. *16*, 432–443.

Callahan, B.J., McMurdie, P.J., Rosen, M.J., Han, A.W., Johnson, A.J., and Holmes, S.P. (2016). DADA2: high-resolution sample inference from Illumina amplicon data. Nat. Methods *13*, 581–583.

Carlens, J., Wahl, B., Ballmaier, M., Bulfone-Paus, S., Förster, R., and Pabst, O. (2009). Common gamma-chain-dependent signals confer selective survival of eosinophils in the murine small intestine. J. Immunol. *183*, 5600–5607.

Chen, Q., Nair, S., and Ruedl, C. (2022). Microbiota regulates the turnover kinetics of gut macrophages in health and inflammation. Life Sci. Alliance *5*, e202101178.

Cherry, W.B., Yoon, J., Bartemes, K.R., Iijima, K., and Kita, H. (2008). A novel IL-1 family cytokine, IL-33, potently activates human eosinophils. J. Allergy Clin. Immunol. *121*, 1484–1490.

Chester, D., and Brown, A.C. (2017). The role of biophysical properties of provisional matrix proteins in wound repair. Matrix Biol. *60–61*, 124–140.

Chiaranunt, P., Tai, S.L., Ngai, L., and Mortha, A. (2021). Beyond immunity: underappreciated functions of intestinal macrophages. Front. Immunol. *12*, 749708.

Chu, D.K., Jimenez-Saiz, R., Verschoor, C.P., Walker, T.D., Goncharova, S., Llop-Guevara, A., Shen, P., Gordon, M.E., Barra, N.G., Bassett, J.D., et al. (2014a). Indigenous enteric eosinophils control DCs to initiate a primary Th2 immune response *in vivo*. J. Exp. Med. *211*, 1657–1672.

Chu, V.T., Beller, A., Rausch, S., Strandmark, J., Zänker, M., Arbach, O., Kruglov, A., and Berek, C. (2014b). Eosinophils promote generation and maintenance of immunoglobulin-A-expressing plasma cells and contribute to gut immune homeostasis. Immunity *40*, 582–593.

Chumakov, A.M., Kubota, T., Walter, S., and Koeffler, H.P. (2004). Identification of murine and human XCP1 genes as C/EBP-epsilon-dependent members of FIZZ/resistin gene family. Oncogene *23*, 3414–3425.

Cox, J., and Mann, M. (2008). MaxQuant enables high peptide identification rates, individualized p.p.b.-range mass accuracies and proteome-wide protein quantification. Nat. Biotechnol. *26*, 1367–1372.

Cox, J., Neuhauser, N., Michalski, A., Scheltema, R.A., Olsen, J.V., and Mann, M. (2011). Andromeda: a peptide search engine integrated into the MaxQuant environment. J. Proteome Res. *10*, 1794–1805.

Dey, N., Wagner, V.E., Blanton, L.V., Cheng, J., Fontana, L., Haque, R., Ahmed, T., and Gordon, J.I. (2015). Regulators of gut motility revealed by a gnotobiotic model of diet-microbiome interactions related to travel. Cell *163*, 95–107.

Drake, M.G., Lebold, K.M., Roth-Carter, Q.R., Pincus, A.B., Blum, E.D., Proskocil, B.J., Jacoby, D.B., Fryer, A.D., and Nie, Z. (2018). Eosinophil and airway nerve interactions in asthma. J. Leukoc. Biol. *104*, 61–67.

FitzPatrick, R.D., Kennedy, M.H.E., Lawrence, K.M., Gauthier, C.M., Moeller, B.E., Robinson, A.N., and Reynolds, L.A. (2020). Littermate-controlled experiments reveal eosinophils are not essential for maintaining steady-state IgA and demonstrate the influence of rearing conditions on antibody phenotypes in eosinophil-deficient mice. Front. Immunol. *11*, 557960.

Flood-Page, P., Menzies-Gow, A., Phipps, S., Ying, S., Wangoo, A., Ludwig, M.S., Barnes, N., Robinson, D., and Kay, A.B. (2003). Anti-IL-5 treatment reduces deposition of ECM proteins in the bronchial subepithelial basement membrane of mild atopic asthmatics. J. Clin. Invest. *112*, 1029–1036.

Fulkerson, P.C., Fischetti, C.A., McBride, M.L., Hassman, L.M., Hogan, S.P., and Rothenberg, M.E. (2006). A central regulatory role for eosinophils and the eotaxin/CCR3 axis in chronic experimental allergic airway inflammation. Proc. Natl. Acad. Sci. USA *103*, 16418–16423.

Goh, Y.P., Henderson, N.C., Heredia, J.E., Red Eagle, A., Odegaard, J.I., Lehwald, N., Nguyen, K.D., Sheppard, D., Mukundan, L., Locksley, R.M., and Chawla, A. (2013). Eosinophils secrete IL-4 to facilitate liver regeneration. Proc. Natl. Acad. Sci. USA. *110*, 9914–9919.

Gombart, A.F., Kwok, S.H., Anderson, K.L., Yamaguchi, Y., Torbett, B.E., and Koeffler, H.P. (2003). Regulation of neutrophil and eosinophil secondary granule gene expression by transcription factors C/EBP epsilon and PU.1. Blood *101*, 3265–3273.

Gouon-Evans, V., Lin, E.Y., and Pollard, J.W. (2002). Requirement of macrophages and eosinophils and their cytokines/chemokines for mammary gland development. Breast Cancer Res. *4*, 155–164.

Gouon-Evans, V., Rothenberg, M.E., and Pollard, J.W. (2000). Postnatal mammary gland development requires macrophages and eosinophils. Development *127*, 2269–2282.

Grisaru-Tal, S., Itan, M., Klion, A.D., and Munitz, A. (2020). A new dawn for eosinophils in the tumour microenvironment. Nat. Rev. Cancer *20*, 594–607.

Griseri, T., Arnold, I.C., Pearson, C., Krausgruber, T., Schiering, C., Franchini, F., Schulthess, J., McKenzie, B.S., Crocker, P.R., and Powrie, F. (2015). Granulocyte macrophage colony-stimulating factor-activated eosinophils promote interleukin-23 driven chronic colitis. Immunity *43*, 187–199.

Groulx, J.F., Gagné, D., Benoit, Y.D., Martel, D., Basora, N., and Beaulieu, J.F. (2011). Collagen VI is a basement membrane component that regulates epithelial cell-fibronectin interactions. Matrix Biol. *30*, 195–206.

Gurtner, A., Borrelli, C., Núñez, N.G., Gonzalez-Perez, I., Crepaz, D., Handler, K., Valenta, T., Basler, K., Becher, B., Moor, A.E., and Arnold, I.C. (2021). Single-cell RNA sequencing unveils intestinal eosinophil development and specialization. Preprint at bioRxiv. 10.27.466053.

Hao, Z., and Rajewsky, K. (2001). Homeostasis of peripheral B cells in the absence of B cell influx from the bone marrow. J. Exp. Med. *194*, 1151–1164.

Hayes, C.L., Dong, J., Galipeau, H.J., Jury, J., McCarville, J., Huang, X., Wang, X.Y., Naidoo, A., Anbazhagan, A.N., Libertucci, J., et al. (2018). Commensal microbiota induces colonic barrier structure and functions that contribute to homeostasis. Sci. Rep. *8*, 14184.

Heath, J.P. (1996). Epithelial cell migration in the intestine. Cell Biol. Int. *20*, 139–146.

Heredia, J.E., Mukundan, L., Chen, F.M., Mueller, A.A., Deo, R.C., Locksley, R.M., Rando, T.A., and Chawla, A. (2013). Type 2 innate signals stimulate fibro/adipogenic progenitors to facilitate muscle regeneration. Cell *153*, 376–388.

Huang, L., and Appleton, J.A. (2016). Eosinophils in helminth infection: defenders and dupes. Trends Parasitol. *32*, 798–807.

Hubbard, B., Buczek-Thomas, J.A., Nugent, M.A., and Smith, M.L. (2014). Heparin-dependent regulation of fibronectin matrix conformation. Matrix Biol. *34*, 124–131.

Humbles, A.A., Lloyd, C.M., McMillan, S.J., Friend, D.S., Xanthou, G., McKenna, E.E., Ghiran, S., Gerard, N.P., Yu, C., Orkin, S.H., and Gerard, C. (2004). A critical role for eosinophils in allergic airways remodeling. Science *305*, 1776–1779.

Ito, M., Hiramatsu, H., Kobayashi, K., Suzue, K., Kawahata, M., Hioki, K., Ueyama, Y., Koyanagi, Y., Sugamura, K., Tsuji, K., et al. (2002). NOD/SCID/gamma(c)(null) mouse: an excellent recipient mouse model for engraftment of human cells. Blood *100*, 3175–3182.

Jacobs, S., Hassell, K., Seston, E., Potter, H., and Schafheutle, E. (2013). Identifying and managing performance concerns in community pharmacists in the UK. J. Health Serv. Res. Policy *18*, 144–150.

Jiménez-Saiz, R., Anipindi, V.C., Galipeau, H., Ellenbogen, Y., Chaudhary, R., Koenig, J.F., Gordon, M.E., Walker, T.D., Mandur, T.S., Abed, S., et al. (2020). Microbial regulation of enteric eosinophils and its impact on tissue remodeling and Th2 immunity. Front. Immunol. *11*, 155.

Johnston, L.K., and Bryce, P.J. (2017). Understanding interleukin 33 and its roles in eosinophil development. Front. Med. (Lausanne) *4*, 51.

Jung, Y., Wen, T., Mingler, M.K., Caldwell, J.M., Wang, Y.H., Chaplin, D.D., Lee, E.H., Jang, M.H., Woo, S.Y., Seoh, J.Y., et al. (2015). IL-1beta in eosinophil-mediated small intestinal homeostasis and IgA production. Mucosal Immunol. *8*, 930–942.

Kang, B., Alvarado, L.J., Kim, T., Lehmann, M.L., Cho, H., He, J., Li, P., Kim, B.H., Larochelle, A., and Kelsall, B.L. (2020). Commensal microbiota drive the functional diversification of colon macrophages. Mucosal Immunol. *13*, 216–229.

Kato, M., Kephart, G.M., Talley, N.J., Wagner, J.M., Sarr, M.G., Bonno, M., McGovern, T.W., and Gleich, G.J. (1998). Eosinophil infiltration and degranulation in normal human tissue. Anat. Rec. *252*, 418–425.

Kawai, T., Adachi, O., Ogawa, T., Takeda, K., and Akira, S. (1999). Unresponsiveness of MyD88-deficient mice to endotoxin. Immunity *11*, 115–122.

Lee, E.H., Itan, M., Jang, J., Gu, H.J., Rozenberg, P., Mingler, M.K., Wen, T., Yoon, J., Park, S.Y., Roh, J.Y., et al. (2018). Eosinophils support adipocyte maturation and promote glucose tolerance in obesity. Sci. Rep. *8*, 9894.

Li, X., Wu, Z., Ni, J., Liu, Y., Meng, J., Yu, W., Nakanishi, H., and Zhou, Y. (2016). Cathepsin B regulates collagen expression by fibroblasts via prolonging TLR2/NF-kappaB activation. Oxid. Med. Cell. Longev. *2016*, 7894247.

Liberzon, A., Birger, C., Thorvaldsdóttir, H., Ghandi, M., Mesirov, J.P., and Tamayo, P. (2015). The Molecular Signatures Database (MSigDB) hallmark gene set collection. Cell Syst. *1*, 417–425.

Loffredo, L.F., Coden, M.E., Jeong, B.M., Walker, M.T., Anekalla, K.R., Doan, T.C., Rodriguez, R., Browning, M., Nam, K., Lee, J.J., et al. (2020). Eosinophil accumulation in postnatal lung is specific to the primary septation phase of development. Sci. Rep. *10*, 4425.

McGuire, J.K., Li, Q., and Parks, W.C. (2003). Matrilysin (matrix metalloproteinase-7) mediates E-cadherin ectodomain shedding in injured lung epithelium. Am. J. Pathol. *162*, 1831–1843.

Mesnil, C., Raulier, S., Paulissen, G., Xiao, X., Birrell, M.A., Pirottin, D., Janss, T., Starkl, P., Ramery, E., Henket, M., et al. (2016). Lung-resident eosinophils represent a distinct regulatory eosinophil subset. J. Clin. Invest. *126*, 3279–3295.

Mishra, A., Hogan, S.P., Lee, J.J., Foster, P.S., and Rothenberg, M.E. (1999). Fundamental signals that regulate eosinophil homing to the gastrointestinal tract. J. Clin. Invest. *103*, 1719–1727.

Miyata, J., Fukunaga, K., Iwamoto, R., Isobe, Y., Niimi, K., Takamiya, R., Takihara, T., Tomomatsu, K., Suzuki, Y., Oguma, T., et al. (2013). Dysregulated synthesis of protectin D1 in eosinophils from patients with severe asthma. J. Allergy Clin. Immunol. *131*, 353–360.e1.

Muller, P.A., Koscsó, B., Rajani, G.M., Stevanovic, K., Berres, M.L., Hashimoto, D., Mortha, A., Leboeuf, M., Li, X.M., Mucida, D., et al. (2014). Crosstalk between muscularis macrophages and enteric neurons regulates gastrointestinal motility. Cell *158*, 300–313.

Naba, A., Clauser, K.R., Ding, H., Whittaker, C.A., Carr, S.A., and Hynes, R.O. (2016). The extracellular matrix: tools and insights for the "omics" era. Matrix Biol. *49*, 10–24.

Naba, A., Clauser, K.R., and Hynes, R.O. (2015). Enrichment of extracellular matrix proteins from tissues and digestion into peptides for mass spectrometry analysis. J. Vis. Exp. *101*, e53057.

Nagase, H., Okugawa, S., Ota, Y., Yamaguchi, M., Tomizawa, H., Matsushima, K., Ohta, K., Yamamoto, K., and Hirai, K. (2003). Expression and function of toll-like receptors in eosinophils: activation by toll-like receptor 7 ligand. J. Immunol. *171*, 3977–3982.

Nowicka, M., Krieg, C., Crowell, H.L., Weber, L.M., Hartmann, F.J., Guglietta, S., Becher, B., Levesque, M.P., and Robinson, M.D. (2017). CyTOF workflow: differential discovery in high-throughput high-dimensional cytometry datasets. F1000Res *6*, 748.

Pinto, S.M., Subbannayya, Y., Rex, D.A.B., Raju, R., Chatterjee, O., Advani, J., Radhakrishnan, A., Keshava Prasad, T.S., Wani, M.R., and Pandey, A. (2018). A network map of IL-33 signaling pathway. J. Cell Commun. Signal. *12*, 615–624.

Plubell, D.L., Wilmarth, P.A., Zhao, Y., Fenton, A.M., Minnier, J., Reddy, A.P., Klimek, J., Yang, X., David, L.L., and Pamir, N. (2017). Extended multiplexing of tandem mass tags (TMT) labeling reveals age and high fat diet specific proteome changes in mouse epididymal adipose tissue. Mol. Cell. Proteomics *16*, 873–890.

Pope, S.M., Zimmermann, N., Stringer, K.F., Karow, M.L., and Rothenberg, M.E. (2005). The eotaxin chemokines and CCR3 are fundamental regulators of allergen-induced pulmonary eosinophilia. J. Immunol. *175*, 5341–5350.

Prochazka, M., Gaskins, H.R., Shultz, L.D., and Leiter, E.H. (1992). The nonobese diabetic scid mouse: model for spontaneous thymomagenesis associated with immunodeficiency. Proc. Natl. Acad. Sci. USA *89*, 3290–3294.

Qiu, Y., Nguyen, K.D., Odegaard, J.I., Cui, X., Tian, X., Locksley, R.M., Palmiter, R.D., and Chawla, A. (2014). Eosinophils and type 2 cytokine signaling in macrophages orchestrate development of functional beige fat. Cell *157*, 1292–1308.

Rappsilber, J., Mann, M., and Ishihama, Y. (2007). Protocol for micro-purification, enrichment, pre-fractionation and storage of peptides for proteomics using StageTips. Nat. Protoc. *2*, 1896–1906.

Ritchie, M.E., Phipson, B., Wu, D., Hu, Y., Law, C.W., Shi, W., and Smyth, G.K. (2015). limma powers differential expression analyses for RNA-sequencing and microarray studies. Nucleic Acids Res. *43*, e47.

Robinson, M.D., McCarthy, D.J., and Smyth, G.K. (2010). edgeR: a Bioconductor package for differential expression analysis of digital gene expression data. Bioinformatics *26*, 139–140.

Rothenberg, M.E., and Hogan, S.P. (2006). The eosinophil. Annu. Rev. Immunol. *24*, 147–174.

Schinke, T., Haberland, M., Jamshidi, A., Nollau, P., Rueger, J.M., and Amling, M. (2004). Cloning and functional characterization of resistin-like molecule gamma. Biochem. Biophys. Res. Commun. *314*, 356–362.

Schneider, C., Rasband, W., and Eliceiri, K. (2012). NIH Image to ImageJ: 25 years of image analysis. Nat Methods *9*, 671–675.

Shah, K., Ignacio, A., McCoy, K.D., and Harris, N.L. (2020). The emerging roles of eosinophils in mucosal homeostasis. Mucosal Immunol. *13*, 574–583.

Shaw, T.N., Houston, S.A., Wemyss, K., Bridgeman, H.M., Barbera, T.A., Zangerle-Murray, T., Strangward, P., Ridley, A.J.L., Wang, P., Tamoutounour, S., et al. (2018). Tissue-resident macrophages in the intestine are long lived and defined by Tim-4 and CD4 expression. J. Exp. Med. *215*, 1507–1518.

Shultz, L.D., Lyons, B.L., Burzenski, L.M., Gott, B., Chen, X., Chaleff, S., Kotb, M., Gillies, S.D., King, M., Mangada, J., et al. (2005). Human lymphoid and myeloid cell development in NOD/LtSz-scid IL2R gamma null mice engrafted with mobilized human hemopoietic stem cells. J. Immunol. *174*, 6477–6489.

Smith, K., McCoy, K.D., and Macpherson, A.J. (2007). Use of axenic animals in studying the adaptation of mammals to their commensal intestinal microbiota. Semin. Immunol. *19*, 59–69.

Sottile, J., and Hocking, D.C. (2002). Fibronectin polymerization regulates the composition and stability of extracellular matrix fibrils and cell-matrix adhesions. Mol. Biol. Cell *13*, 3546–3559.

Sugawara, R., Lee, E.J., Jang, M.S., Jeun, E.J., Hong, C.P., Kim, J.H., Park, A., Yun, C.H., Hong, S.W., Kim, Y.M., et al. (2016). Small intestinal eosinophils regulate Th17 cells by producing IL-1 receptor antagonist. J. Exp. Med. *213*, 555–567.

Suzukawa, M., Koketsu, R., Iikura, M., Nakae, S., Matsumoto, K., Nagase, H., Saito, H., Matsushima, K., Ohta, K., Yamamoto, K., and Yamaguchi, M. (2008). Interleukin-33 enhances adhesion, CD11b expression and survival in human eosinophils. Lab. Invest. *88*, 1245–1253.

Swartz, J.M., Byström, J., Dyer, K.D., Nitto, T., Wynn, T.A., and Rosenberg, H.F. (2004). Plasminogen activator inhibitor-2 (PAI-2) in eosinophilic leukocytes. J. Leukoc. Biol. *76*, 812–819.

Uderhardt, S., Ackermann, J.A., Fillep, T., Hammond, V.J., Willeit, J., Santer, P., Mayr, M., Biburger, M., Miller, M., Zellner, K.R., et al. (2017). Enzymatic lipid oxidation by eosinophils propagates coagulation, hemostasis, and thrombotic disease. J. Exp. Med. *214*, 2121–2138.

van Tol, E.A., Holt, L., Li, F.L., Kong, F.M., Rippe, R., Yamauchi, M., Pucilowska, J., Lund, P.K., and Sartor, R.B. (1999). Bacterial cell wall polymers promote intestinal fibrosis by direct stimulation of myofibroblasts. Am. J. Physiol. *277*, G245–G255.

Vicetti Miguel, R.D., Quispe Calla, N.E., Dixon, D., Foster, R.A., Gambotto, A., Pavelko, S.D., Hall-Stoodley, L., and Cherpes, T.L. (2017). IL-4-secreting eosinophils promote endometrial stromal cell proliferation and prevent Chlamydia-induced upper genital tract damage. Proc. Natl. Acad. Sci. USA *114*, E6892–E6901.

Vllasaliu, D., Falcone, F.H., Stolnik, S., and Garnett, M. (2014). Basement membrane influences intestinal epithelial cell growth and presents a barrier to the movement of macromolecules. Exp. Cell Res. *323*, 218–231.

Wang, H., Foong, J.P.P., Harris, N.L., and Bornstein, J.C. (2022). Enteric neuroimmune interactions coordinate intestinal responses in health and disease. Mucosal Immunol. *15*, 27–39.

Weller, P.F., and Spencer, L.A. (2017). Functions of tissue-resident eosinophils. Nat. Rev. Immunol. *17*, 746–760.

Westermann, S., Dietschmann, A., Doehler, D., Castiglione, K., Bochner, B.S., Voehringer, D., and Radtke, D. (2022). Siglec-F promotes IL-33-induced cytokine release from bone marrow-derived eosinophils independently of the ITIM and ITIM-like motif phosphorylation. J. Immunol. *208*, 732–744.

Wu, D., Molofsky, A.B., Liang, H.E., Ricardo-Gonzalez, R.R., Jouihan, H.A., Bando, J.K., Chawla, A., and Locksley, R.M. (2011). Eosinophils sustain

adipose alternatively activated macrophages associated with glucose homeostasis. Science *332*, 243–247.

Xenakis, J.J., Howard, E.D., Smith, K.M., Olbrich, C.L., Huang, Y., Anketell, D., Maldonado, S., Cornwell, E.W., and Spencer, L.A. (2018). Resident intestinal eosinophils constitutively express antigen presentation markers and include two phenotypically distinct subsets of eosinophils. Immunology *154*, 298–308.

Yu, C., Cantor, A.B., Yang, H., Browne, C., Wells, R.A., Fujiwara, Y., and Orkin, S.H. (2002). Targeted deletion of a high-affinity GATA-binding site in the GATA-1 promoter leads to selective loss of the eosinophil lineage *in vivo*. J. Exp. Med. *195*, 1387–1395.

Zeng, M.Y., Cisalpino, D., Varadarajan, S., Hellman, J., Warren, H.S., Cascalho, M., Inohara, N., and Núñez, G. (2016). Gut microbiota-induced immunoglobulin G controls systemic infection by symbiotic bacteria and pathogens. Immunity *44*, 647–658.

Zudaire, E., Gambardella, L., Kurcz, C., and Vermeren, S. (2011). A computational tool for quantitative analysis of vascular networks. PLoS One *6*, e27385.

Please cite this article in press as: Ignacio et al., Small intestinal resident eosinophils maintain gut homeostasis following microbial colonization, Immunity (2022), https://doi.org/10.1016/j.immuni.2022.05.014





## STAR★METHODS

### KEY RESOURCES TABLE

| REAGENT or RESOURCE | SOURCE | IDENTIFIER |
|---|---|---|
| Antibodies | | |
| V450 anti-mouse CD45 (30-F11) | BD | Cat# 560501; RRID:AB_1645275 |
| BV510 anti-mouse CD45 (30-F11) | BD | Cat# 563891; RRID:AB_2734134 |
| FITC anti-mouse CD45 (30-F11) | BD | Cat# 561088; RRID:AB_10562038 |
| BV605 anti-mouse Siglec-F (E50-2440) | BD | Cat# 740388; RRID:AB_2740118 |
| PE anti-mouse Siglec-F (E50-2440) | BD | Cat# 552126; RRID:AB_394341 |
| FITC anti-mouse CD11b (M1/70) | BD | Cat# 553310; RRID:AB_394774 |
| APC-Cy7 anti-mouse CD11b (M1/70) | BD | Cat# 557657; RRID:AB_396772 |
| PeCy7 anti-mouse CD11c (HL3) | BD | Cat# 558079; RRID:AB_647251 |
| AF700 anti-mouse Ly6C (HK1.4) | Biolegend | Cat# 128024; RRID:AB_10643270 |
| BV510 anti-mouse I-A/I-E (M5/114-15-2) | BD | Cat# 742893; RRID:AB_2741133 |
| PE anti-mouse CD103 (3E7) | Biolegend | Cat# 121406; RRID:AB_1133989 |
| PerCP-Cy5.5 anti-mouse Ly6G and Ly6C (Gr1) (RB68C5) | BD | Cat# 552093; RRID:AB_394334 |
| Biotin anti-mouse CD193 (CCR3) Clone J073E5 | Biolegend | Cat# 144520; RRID:AB_2632633 |
| BV421 anti-mouse CD44 (IM7) | BD | Cat# 563970; RRID:AB_2738517 |
| AF647 anti-CD64 (X54-5/7.1) | BD | Cat# 558539; RRID:AB_647120 |
| PerCP-Cy5.5 anti-mouse CD19 (1D3) | BD | Cat# 551001; RRID:AB_394004 |
| PerCP-Cy5.5 anti-mouse CD3e (145-2C11) | BD | Cat# 551163; RRID:AB_394082 |
| PerCP-Cy5.5 anti-mouse Ly6G (1A8) | BD | Cat# 560602; RRID:AB_1727563 |
| APC anti-mouse IgG1 (A85-1) | BD | Cat# 560089; RRID:AB_1645625 |
| BV786 anti-mouse IgG2b (R12-3) | BD | Cat# 743179; RRID:AB_2741330 |
| BV421 anti-mouse IgG2a/c (RMG2a-62) | Biolegend | Cat# 407117; RRID:AB_2687343 |
| BV605 anti-mouse IgG3 (R40-82) | BD | Cat# 744135; RRID:AB_2742024 |
| PE anti-mouse IgM (R6-60.2) | BD | Cat# 562033; RRID:AB_10896320 |
| PerCP-Cy5.5 Mouse anti-BrdU (3D4) | BD | Cat# 560809; RRID:AB_2033929 |
| 89Y anti-mouse CD45 (30-F11) | Fluidigm | Cat# 3089005B; RRID:AB_2651152 |
| 174Yb anti-mouse Ly6G and Ly6C/Gr1 (RB68C5) | Fluidigm | Cat# 3174008B |
| 209Bi anti-mouse CD11c (N418) | Fluidigm | Cat# 3209005B; RRID:AB_2811244 |
| 162Dy Purified anti-mouse Ly6C (HK1.4) | Biolegend/self-labelled | Cat# 128039; RRID:AB_2563783 |
| 159Tb Purified anti-mouse F4/80 (BM8) | Biolegend/self-labelled | Cat# 123143; RRID:AB_2563767 |
| 154Sm Purified anti-mouse CD11b (M1/70) | Biolegend/self-labelled | Cat# 101248; RRID:AB_2561479 |
| 155Gd Purified anti-mouse Siglec-F(E50-2440) | BD/self-labelled | Cat# 552125; RRID:AB_394340 |
| 176Yb Purified anti-mouse CCR3 (J073E5) | Novus Biologicals/self-labelled | Cat# MAB1551-100; RRID:AB_2074150 |
| 142Nd Purified anti-mouse IL33Ra/ST2 (DIH9) | Biolegend/self-labelled | Cat# 145302; RRID:AB_2561843 |
| 144Nd Purified anti-mouse B220 (RA3-6B2) | Fluidigm | Cat# 3144011B; RRID:AB_2811239 |
| 145Nd Purified anti-mouse CD4 (RM4-5) | Fluidigm | Cat# 3145002B; RRID:AB_2687832 |
| 144Sm Purified anti-mouse I-A/I-E (m5/114.15.2) | Biolegend/self-labelled | Cat# 107637; RRID:AB_2563771 |
| 149Sm Purified anti-mouse CD19 (6D5) | Fluidigm | Cat# 3149002B; RRID:AB_2814679 |
| 152Sm Purified anti-mouse CD3e (145-2C11) | Fluidigm | Cat# 3152004B; RRID:AB_2687836 |
| 153Eu Purified anti-mouse CD8a (53-6.7) | Fluidigm | Cat# 3153012B; RRID:AB_2885019 |
| 161Dy Purified anti-mouse CD138 (281-2) | Biolegend/self-labelled | Cat# 142502; RRID:AB_10965646 |
| 163Dy Purified anti-mouse CD335 (29A1.4) | Biolegend/self-labelled | Cat# 137625; RRID:AB_2563744 |
| 164Dy Purified anti-mouse CX3CR1 (SA011F11) | Fluidigm | Cat# 3164023B; RRID:AB_2832247 |
| 166Er Purified anti-mouse CD103 (2E7) | Biolegend/self-labelled | Cat# 121402; RRID:AB_535945 |

(*Continued on next page*)

Please cite this article in press as: Ignacio et al., Small intestinal resident eosinophils maintain gut homeostasis following microbial colonization, Immunity (2022), https://doi.org/10.1016/j.immuni.2022.05.014



*Continued*

| REAGENT or RESOURCE | SOURCE | IDENTIFIER |
|---|---|---|
| 170Er Purified anti-mouse CD161 (PK136) | Fluidigm | Cat# 3170002B; RRID:AB_2885023 |
| 171Yb Purified anti-mouse CD64 (X54-5/7.1) | Biolegend/self-labelled | Cat# 139302; RRID:AB_10613107 |
| 175Lu Purified anti-mouse CD127 (A7R34) | Fluidigm | Cat# 3175006B |
| GP38/Podoplanin (PE, 8.1.1) | Biolegend | Cat# 127408; RRID:AB_2161928 |
| CD31/Pecam-1 (PE-Cy7, clone: 390) | BD Biosciences | Cat# 561410; RRID:AB_10612003 |
| Lyve-1 | ReliaTech GmbH | Cat# 103-PA50; RRID:AB_2783787 |
| VEGFR2/KDR/Flk-1 (clone: AF644) | RND Systems | Cat# AF644; RRID:AB_355500 |
| E-cadherin (clone: 36/E-cadherin) | BD Biosciences | Cat# 610181; RRID:AB_397580 |
| GFAP | Dako | Cat# Z0334; RRID:AB_10013382 |
| α-SMA (Cy3, clone: 1A4) | Sigma | Cat# C6198; RRID:AB_476856 |
| DCAMKL1 | Abcam | Cat# ab31704; RRID:AB_873537 |
| Lysozyme (clone: EC 3.2.1.17) | Dako | Cat# A0099; RRID:AB_2756949 |
| E-cadherin | RND Systems | Cat# AF748; RRID:AB_355568 |
| Ki67 (clone: sp6) | Spring amsbio | Cat# M3060; RRID:AB_1661313 |
| Donkey anti-mouse IgG (H+L) secondary Ab (AlexaFluor 555) | Life Technologies | Cat# A31570; RRID:AB_2536180 |
| Chicken anti-rat IgG (H+L) secondary Ab (AlexaFluor 647) | Life Technologies | Cat# A21472; RRID:AB_2535875 |
| Donkey anti-rat IgG (H+L) secondary Ab (AlexaFluor488) | Life Technologies | Cat# A21208; RRID:AB_2535794 |
| Donkey anti-goat IgG (H+L) secondary Ab (AlexaFluor647) | Life Technologies | Cat# A21447; RRID:AB_2535864 |
| **Bacterial and virus strains** | | |
| *Akkermansia muciniphila* YL44 | DSM | DSM 26127 |
| **Chemicals, peptides, and recombinant proteins** | | |
| Sodium dodecyl sulfate (SDS) | VWR | Cat# CA71007-096 |
| Dithiothreitol (DTT) | GoldBio | Cat# DTT25 |
| 4-(2-hydroxyethyl)-1-piperazineethanesulfonic acid (HEPES) | VWR | Cat#0511-250g |
| Protease Inhibitor Cocktail | Roche | Cat#11873580001 |
| Guanidine hydrochloride | VWR | Cat#0287-500g |
| Iodoacetamide | GE Healthcare | Cat#RPN6302 |
| Heavy Formaldehyde (13CD2O) | Cambridge Isotope Laboratories | Cat#CDLM-4559-1 |
| Formaldehyde (CH2O) | VWR | Cat#41860-360 |
| Sodium cyanoborohydride | MilliporeSigma | Cat# Ca8.18053.0010 |
| Trypsin | Promega | Cat# V5280 |
| Trifluoracetic acid | Fisher Chemical | Cat# A116-50 |
| HiPerSolv/super gradient grade | VWR | Cat# BDH83639.100E |
| Formic Acid | Fisher Chemical | Cat# A117-50 |
| APC Streptavidin | Biolegend | Cat# 405207 |
| PerCP-Cy5.5 Streptavidin | Biolegend | Cat# 405214 |
| Fixable Viability Stain 780 | BD | Cat# 565388 |
| Liberase TL Research Grade | Roche | Cat# 5401020001 |
| DNase I recombinant | Roche | Cat# 4536282001 |
| o-Phenylenediamine | Sigma | Cat# P9029-50G |
| Tris-base | N/A | N/A |
| Hydrogen peroxide solution | Sigma | Cat# H3410-500ML |
| Ethylenediaminetetraacetic acid | Sigma | Cat# 431788-100G |
| RPMI 1640 Medium, no phenol red | Gibco | Cat# 11835030 |
| HyClone RPMI 1640 Media | GE Healthcare Cell Culture | Cat# SH30027FS |

(*Continued on next page*)

*Continued*

| REAGENT or RESOURCE | SOURCE | IDENTIFIER |
|---|---|---|
| HyClone HEPES 1M Solution | GE Healthcare Cell Culture | Cat# SH30237.01 |
| Fluorescein isothiocyanate–dextran, 4kDa | Sigma | Cat# 46944-100MG-F |
| Carmine, powder | Sigma | Cat# C1022-5G |
| Methyl cellulose, 400cP | Sigma | Cat# M0262-100G |
| BrdU (5-Bromo-2′-deoxyuridine) | Sigma | Cat# 19-160 |
| Mucin from porcine stomach, Type II | Sigma | Cat# M2378-100G |
| Sodium azide | Sigma | Cat# S2002-100G |
| Bovine Serum Albumin | Sigma | Cat# A7030-500G |
| Saponin | Sigma | Cat# 84510-100G |
| Glutaraldehyde fixative | Agar Scientific | Cat# AGR1009 |
| KAPA HiFi Hot Start Ready Mix | Roche | Cat# KK2602 |
| NucleoMag NGS clean-up beads | Macherey-Nagel | Cat# 744970.50 |
| Cisplatin | BioVision | Cat# 1550-1000 |
| Iridium | Fluidigm | Cat# 201192B |
| EQ Four Element Calibration Beads | Fluidigm | Cat# 201078 |
| Maxpar Cell Acquisition Solution | Fluidigm | Cat# 201240 |
| SPI-Chem Osmium Tetroxide | SPI Supplies | Cat# 20816-12-0 |
| Trizma maleate buffer | Sigma | Cat# 913-50ML |
| Epoxy embedding medium | Sigma | Cat# 45345 |
| Toluidine Blue | Sigma | Cat# 89640 |
| Purified Rat Anti-Mouse CD16/CD32 (Mouse BD Fc Block) (2.4G2) | BD | Cat# 553141 |
| EdU (5-ethynyl-2'- deoxyuridine) | ThermoScientific | Cat# A10044 |
| ProLong Gold Antifade Reagent | Invitrogen | Cat# P36934 |
| FocusClear | CellExplorer | Cat# FC-101 |
| Liberase TL | Roche | Cat# 5401020001 |
| DNaseI | Roche | Cat# 04536282001 |
| Bactrim (oral suspension) | Bayer | Cat# SAP-10068284 |
| Dafalgan/Paracetamol | Bayer | Cat# N02BE01 |
| Sodium Chloride | Sigma Aldrich | 71382-1KG |
| Potassium Chloride | Sigma Aldrich | 60130-1KG |
| Potassium phosphate monobasic | Sigma Aldrich | 60218-1KG |
| Magnesium sulfate heptahydrate | Sigma Aldrich | 63140-1KG-F |
| D(+) Glucose | Sigma Aldrich | G7021-1KG |
| Sodium bicarbonate | Sigma Aldrich | S8875-1KG |
| Calcium chloride dihydrate | Sigma Aldrich | C7902-1KG |
| Acetylcholine chloride | Sigma Aldrich | A2661-25G |
| Recombinant Murine Stem Cell Factor | PeproTech | 250-03 |
| Recombinant Murine FLT-3 Ligand | PeproTech | 250-31L |
| Recombinant Murine IL-5 | PeproTech | 215-15 |
| IMDM with Glutamax-I | Life Technologies, Invitrogen | 31980-097 |
| Diff-Quick Stain Kit | Thermo Fisher Scientific | 23-122-929, 23-122-952, and 23-122-937) |
| Olive Oil | Sigma | O1514 |
| **Critical commercial assays** | | |
| Mouse Isotyping Panel 1 kit | Meso Scale Discovery | Cat# K15183B-2 |
| SequalPrep Normalization Plate Kit | Invitrogen | Cat# A10510-01 |
| Qubit HS DNA kit | Invitrogen | Cat# Q33230 |
| Tapestation D1000 assay | Agilent | Cat# G2991AA |
| V2-500 cycle kit | Illumina | Cat# MS-102-2003 |

(*Continued on next page*)

Please cite this article in press as: Ignacio et al., Small intestinal resident eosinophils maintain gut homeostasis following microbial colonization, Immunity (2022), https://doi.org/10.1016/j.immuni.2022.05.014



*Continued*

| REAGENT or RESOURCE | SOURCE | IDENTIFIER |
|---|---|---|
| MaxPar Antibody Labeling kit | Fluidigm | Cat# 201300 |
| Click-iT® Plus EdU Alexa Fluor® 555 Imaging Kit | ThermoScientific | Cat # C10638 |
| RNeasy Plus Universal Mini Kit | Qiagen | Cat# 73404 |
| RNase-Free DNase Set | Qiagen | Cat# 79254 |
| TruSeq Stranded mRNA | Illumina | Cat# 20020594 |
| NextSeq 500/550 High Output v2 kit (75 cycles) | Illumina | FC-404-2005 |
| KAPA RNA HyperPrep Kit with RiboErase (HMR) | KAPA Biosystems | KK8560 |
| QIAamp DNA stool mini kit | Qiagen | 51504 |
| a-CD90.2 Microbeads (T-cell depletion) | Milteny Biotech | Cat. 130-049-101 |
| Anti-Siglec-F MicroBeads, mouse | Miltenyi Biotec | 130-118-513 |
| **Deposited data** | | |
| TMT data | This paper | Pride: PXD033288 |
| Proteomic data shown in Figure S6G | This paper | ProteomeXchange: PXD032084 |
| Microbiome 16S rRNA gene sequences - MiSEQ | This paper | NCBI BioProject: PRJNA832754 |
| Microbiome 16S rRNA gene sequences – Ion Torrent | This paper | NCBI BioProject: PRJNA832494 |
| RNAseq data | This paper | GEO: GSE201355 |
| **Experimental models: Organisms/strains** | | |
| C57BL/6J | Jackson Laboratory | JAX Stock:000664 |
| BALB/cJ | In-house breeding | JAX Stock: 000651 |
| Δdbl.GATA1 | In-house breeding | Yu et al. (2002); JAX Stock: 005653 |
| NOD.SCIDxγc | In-house breeding | Schultz et al. (2005); JAX Stock: 005507 |
| NOD.SCID | In-house breeding | Prochazka et al. (1992); JAX Stock: 001303 |
| *Rag2*ko | Jackson Laboratory | Hao and Rajewsky (2001); JAX Stock: 008449 |
| Myd88-/- | In-house breeding | Adachi et al. (1998) |
| *ST2*$^{-/-}$*xIL17rb*$^{-/-}$ | In-house breeding | JAX Stock: 4457616 X 2386675 |
| **Oligonucleotides** | | |
| 5′AATGATACGGCGACCACCGAGA TCTACAC i5BARCODE TATGGTAATT GTGTGCCAGCMGCCGCGGTAA-3′ | IDT | N/A |
| 5′-CAAGCAGAAGACGGCATACG AGAT i7BARCODE AGTCAGTCAGC CGGACTACHVGGGTWTCTAAT-3′ | IDT | N/A |
| **Software and algorithms** | | |
| Andromeda algorithm | ACS Publications | https://pubs.acs.org/doi/10.1021/pr101065j |
| MaxQuant software package v.1.6.0.1 | MaxQuant | https://www.maxquant.org/ |
| Graphpad Prism | Graphpad | https://www.graphpad.com/ |
| FlowJo | FlowJo | https://www.flowjo.com |
| Image analysis software iTEM | iTEM | http://www.resaltatech.com/item_overview.htm |
| ImageJ | Schneider et al., 2012 | https://imagej.nih.gov/ij/ |
| Angiotool | Zudaire et al., 2011 | A computational tool for quantitative analysis of vascular networks. Zudaire E, Gambardella L, Kurcz C, Vermeren S. PLoS One. 2011;6(11):e27385. Epub 2011 Nov 16. |
| Labchart software (AD Instruments) | N/A | N/A |

(*Continued on next page*)

*Continued*

| REAGENT or RESOURCE | SOURCE | IDENTIFIER |
|---|---|---|
| RNASik v1.4.7 | N/A | https://monashbioinformaticsplatform.github.io/RNAsik-pipe/ |
| Molecular Signature database (Broad Institute; curated gene set collections | Liberzon et al., 2015 | https://www.gsea-msigdb.org/gsea/msigdb/annotate.jsp |
| Diffcyt R package | Diffcyt | https://www.bioconductor.org/packages/release/bioc/html/diffcyt.html |
| CATALYST R package | CATALYST | https://www.bioconductor.org/packages/release/bioc/html/CATALYST.html |
| Other | | |
| 10 kDa cutoff membranes | Amicon, Millipore | Cat# ACS501024 |
| C18 HPLC Columns | Thermo Scientific | Cat# 164569 |
| Sep-Pak plus c18 Cartridges | Waters | Cat#WAT020515 |
| DIO (VHFD) 60 kcal% fat (High-fat diet pellet) | Research Diets | D12492 |
| Control (LFD) 10 kcal% fat D12492 Match 7% Sucrose | Research Diets | D12450J |

## RESOURCE AVAILABILITY

### Lead contact

Further information and requests for resources and reagents should be directed to and will be fulfilled by the lead contact, Dr. Kathy McCoy (kathy.mccoy@ucalgary.ca).

### Materials availability

This study did not generate new unique reagents.

### Data and code availability

- The published article includes all transcriptomic and proteomic datasets in Tables S1, S2, S3, S4, and S5 generated or analysed during this study.
- RNA-seq data have been deposited at GEO and are publicly available as of the date of publication. Accession numbers are listed in the key resources table.
- 16S rRNA amplicon sequences have been deposited in the NCBI BioProject database and are publicly available as of the date of publication. Accession numbers are listed in the key resources table.
- Proteomic data shown in Figure S6G have been deposited at ProteomeXchange and are publicly available as of the date of publication. Accession number is listed in the key resources table.
- TMT data have been deposited at Pride and are publicly available as of the date of publication. Accession number is listed in the key resources table.
- This project does not report original code.
- Any additional information required to reanalyze the data reported in this paper is available from the lead contact upon request.

## EXPERIMENTAL MODEL AND SUBJECT DETAILS

### Mice

For experiments conducted at EPFL, BALB/cJ and ΔdblGATA1 mice sourced from Charles River and Jackson Laboratories respectively, were both rederived and bred under specific pathogen-free (SPF) conditions at the EPFL animal facility. Germ-free (GF) BALB/cJ and ΔdblGATA1 mice used for histological and immunological analysis, alongside re-colonization experiments conducted at EPFL, were bred and sourced from the Clean Mouse Facility (CMF), University of Bern. For re-colonization experiments conducted at EPFL, GF mice of both genotypes received fecal transfers (via oral gavage) from the same SPF BALB/c donor mice and were analyzed at least 4-weeks post-recolonization. $Rag2^{-/-}$ mice (Hao and Rajewsky, 2001) and C57BL/6J mice used as experimental controls were both obtained from Jackson laboratories. NOD.SCID (Prochazka et al., 1992) and NOD.SCID.$\gamma c^{-/-}$ (Shultz et al., 2005) mice were bred and maintained under SPF conditions at the University of Lausanne (UNIL). *Myd88*$^{-/-}$ mice (Adachi et al., 1998) were also bred and maintained at UNIL and were a kind gift from Dr. Sanjiv Luther. *ST2*$^{-/-}$*xIL17rb*$^{-/-}$ mice were donated from B. Marsland Lab (UNIL) and co-housed with BALB/cJ mice (EPFL bred in house) for at least 2 weeks prior to experiments under SPF conditions. For GF and re-colonization experiments conducted at the University of Calgary, all mice were re-derived to germ-free status via two-cell embryo transfer. Mice were bred and maintained at the International Microbiome Centre (IMC),

Please cite this article in press as: Ignacio et al., Small intestinal resident eosinophils maintain gut homeostasis following microbial colonization, Immunity (2022), https://doi.org/10.1016/j.immuni.2022.05.014



University of Calgary, Canada. GF status was routinely monitored by culture-dependent and -independent methods. For recolonization experiments, GF mice were co-housed with a female, aged-matched SPF BALB/c mouse for two weeks in the Mouse Barrier Unit (MBU), University of Calgary, Canada. Intestinal contractility experiments were conducted in Monash University on BALB/cJ and ΔdblGATA1 mice maintained under SPF conditions at the Monash Intensive Care Unit Animal Facility at Monash University, Melbourne, Australia. All mice were age and sex-matched and used between 8-12 weeks of age. Mice were maintained at 3-5 animals per cage and provided *ad libidum* access to water and food. For experiments conducted in EPFL and Monash, soiled cage bedding was mixed weekly and distributed among cages for at least 3 weeks prior to the study to minimize cage-effects and allow for normalization of microbiota. All mice were confirmed to be specific pathogen-free. All the experiments were performed according to the Swiss Animal Welfare, Monash University Animal Ethics Committee (AEC) approvals (Ethics No. E/1828/2018/M) and Canadian Council for Animal Care under protocols (AC17-0090 and AC17-0011) approved by the University of Calgary Health Sciences Animal Care Committee.

## METHOD DETAILS

### Wholemount imaging

Wholemount tissue preparation was conducted according to published protocols (Bernier-Latmani and Petrova, 2016). Tissues for wholemount imaging were collected and regions were divided as follows: first the SI length was measured with the duodenum identified as the first 5 cm of the SI. The remaining tissue was cut in half, with the proximal half identified as the Jejunum and the distal as the ileum. The proximal and distal ends of the jejunum and ileum, alongside the proximal duodenum were used for WM imaging. Regions of interest were collected and pinned onto a silicone-lined plate using metallic (insect) pins to maximize surface area and allow for optimal fixation. All incubations were done at 4C on an orbital shaker. Tissues were fixed overnight with wholemount fixation buffer (0.5% PFA, 15% Picric Acid saturated in 10mM of phosphate buffer (pH 7)). Samples were then washed 1xPBS 5 times, over 10 min intervals. The tissue was then subjected to a sucrose gradient for better preservation of tissue structure/morphology - where the tissues were first incubated with 10% sucrose in 1xPBS for 4hours, then switched to a solution consisting of 20% sucrose 10% glycerol in 1x PBS O/N. Samples were rinsed with 1xPBS at least twice after the O/N incubation. 1-2cm sized tissues were acquired from regions of interest and were pinned on a new silicone-lined plate. Prior to staining, the samples were incubated for at least 4hours with filtered blocking solution (0.5% BSA, 0.1% NaN3, 5% donkey serum, 0.3% Triton-X100 – in 500ml of PBS). Primary antibody incubation was done over 2 days. Post-incubation, the samples were washed with washing buffer (0.03% Triton-X100 in 1xPBS) repeated 5 times over 1hour intervals. Secondary antibodies were incubated O/N, and the plate was covered with aluminum foil to prevent bleaching of conjugated fluorophores. Antibodies were diluted in wholemount blocking buffer. Post-incubation, the samples were washed with washing buffer (0.03% Triton-X100 in 1xPBS) repeated 10 times over 30 min intervals. The samples were then fixed over 2-3 days in 4% PFA. For imaging, tissue was longitudinally cut with scissors into sections approximately 1-2 villi thick (at least 10 strips were obtained per sample). The cut sections were placed on a super-frost slide (after addition of tissue spacers) and the tissue was clarified with FocusClear for 30mins at room temp. After removal of excess FocusClear solution, 1-2 drops of Prolong gold was added – followed by coverslip. The samples were imaged using Zeiss LSM700 (inverted microscope). Villi used for analyses were randomly selected from different regions of the slide. Every image has a field of area containing at least 3 villi, and 10 images were collected per mouse. Images were analyzed using ImageJ/FIJI software, and surface area was traced-manually – but measured by the software. Villus vessel length and branching quantifications were performed by drawing vessel network overlays with Photoshop and exporting these images to Angiotool for quantification (Zudaire et al., 2011).

### Histological analysis using IHC and IF

After collection of tissue for wholemount preparation, the rest of the small intestine reserved for other histological analyses were laid flat (villi-side up) on Whatman paper to maximize surface area for fixation in 4% PFA O/N. The samples were then rolled into 'Swiss rolls' embedded into a cassette, and placed in 70% EtOH. The samples were then prepared for paraffin embedding, and placed into paraffin blocks. 0.4μm sections were sectioned using a microtome (Hyrax M25) and placed onto a super frost slide (2 sections/slide – 1 for negative staining control, 1 test sample). For IHC staining, paraffin sections samples were dewaxed and rehydrated. For antigen retrieval, the samples were incubated with Sodium Citrate Buffer (pH 6) for 5 mins at boiling point, using a standard microwave. After blocking for 1h with wholemount blocking buffer, the primary antibodies were incubated overnight at 4C. After washing with wholemount wash buffer, slides were incubated for 2 hours with secondary antibodies. Antibodies were diluted in wholemount fixation buffer. Slides were counterstained with DAPI for nuclear staining, and mounted with Prolong gold. IF stained slides were imaged with Olympus AX70 fluorescence microscope; on occasion, with Zeiss LSM700 (inverted microscope). For experiments labelling proliferating cells using EdU, mice were injected with EdU (200μg/mouse), 24 hours prior to analysis in a temporally staggered manner to maintain accuracy for the measurement of epithelial migration from villus-crypt axis. To detect cellular EdU-incorporation in paraffin embedded tissues, Click-it EdU kit (Invitrogen) was used according to manufacturer's instructions. Proliferation analysis using Ki67 (rabbit α-Ki67, SP6, Springbio, diluted 1:100) was performed using the fully automated Ventana Discovery ULTRA (Roche Diagnostics, Rotkreuz, Switzerland). Briefly, dewaxed and rehydrated paraffin sections were pretreated with heat using standard condition (40 minutes). The primary antibodies were incubated 1 hour at 37°C. After incubation with a rabbit Immpress HRP (Ready to use, Vector laboratories Laboratories), chromogenic revelation was performed with ChromoMap DAB kit (Roche Diagnostics, Rotkreuz, Switzerland). To identify goblet cells, sections were stained with Periodic-Schiff Stain (PAS). Sections

were counterstained with Harris hematoxylin and permanently mounted. For analysis of both IF and IHC stained samples, at least 10 images were acquired per mouse, with at least 4 villi per field – blindly sampled from different areas of the swiss roll (proximal jejunum). All statistical tests, and graphs were generated using GraphPad Prism.

### RNA-seq experiment

RNA-seq analysis on the small intestine was conducted from tissue acquired from the epithelial-cells and epithelial-depleted (post-epithelial removal; IEC-neg) tissue from the proximal jejunum. Samples were quickly snap frozen in liquid nitrogen until RNA-extraction. RNA- extraction was conducted using QIAGEN RNA-easy universal kit – as per manufacturer's instructions, with an additional DNA-removal step using DNAseI (QIAGEN). Samples were stored at -80C until further analysis. Multiplexed libraries for mRNA-seq were prepared according to manufacturer's instructions with the TruSeq stranded mRNA kit (Illumina) starting from 3000 ng of good-quality total RNAs (RNA quality scores >7.5 on the TapeStation 4200). Libraries were subsequently loaded at 1.44pM on a High Output flow cell (Illumina) and sequenced in a NextSeq 500 instrument (Illumina) according to manufacturer instructions, yielding single-end reads of 75 nucleotides. Multiplexed libraries for total RNA-seq were prepared according to manufacturer's instructions with the "RNA HyperPrep with RiboErase" kit (Kapa) starting from 200 ng of total RNAs. Since RNA quality varied among samples (scores from 4.1 to 8.3 on the TapeStation 4200), RNA fragmentation times were adjusted as recommended by the manufacturer. Libraries were subsequently pooled and loaded at 1.53pM on two High Output flow cells (Illumina) and sequenced in a NextSeq 500 instrument (Illumina) according to manufacturer instructions, yielding single-end reads of 75 nucleotides. Reads from these two runs were then pooled. Raw fastq files were processed using RNASik v1.4.7 with default settings (https://monashbioinformaticsplatform.github.io/RNAsik-pipe/). RNASik wraps alignment, QC metrics and quantification in the one script giving a count file. Alignment was performed using STAR v2.5.2 against iGenomes ensembl GRCm10 reference. Using the GTF from the same reference, FeatureCounts quantified reads to genes. Data was uploaded onto Degust (https://doi.org/10.5281/zenodo.3258932) for RNA-seq qanalysis and visualization. Differentially expressed genes (DEGs) were normalized using EdgeR method in Degust, and were identified using $\log_2$FC > 1, FDR cut-off >0.01. For GSEA analysis, identified DEGs were analyzed using the Molecular Signature database (Broad Institute; curated gene set collections) (Liberzon et al., 2015).

### Chimera experiment

For chimera experiments, 8–12-week-old mice were pre-treated with antibiotics (Bactrim) in their drinking water for 2 days prior to the irradiation. The mice were then lethally irradiated with a total of exposure of 700 gray – split into two doses (335gy per dose), 12 hours apart. After the last dose, the hematopoietic compartment for each irradiated mouse (recipient) was reconstituted with approx. 7-10 x10^6 cells from donor mice (6-8 weeks old) after pan-T cell depletion (a-CD90.2, Milteny Biotech Cat. 130-049-101) following manufacturer's instructions. All steps were conducted on ice, in a sterile hood. From day -2 till week 6, the mice were kept on antibiotics and analgesics (Dafalgan). 24 hours prior to analysis, the mice were injected with EdU (200μg/mouse), in a temporally staggered manner to maintain accuracy for proliferation studies. For Click-it EdU staining, protocol was followed according to manufacturer's instructions. The mice were analyzed 4 weeks after antibiotic removal.

### Quantitative mass spectrometry of ECM-enriched fraction

ECM-enriched fraction was obtained from the proximal jejunum following a decellularization procedure using the Compartment Protein Extraction kit (Merck Millipore) and were digested into peptides using a method previously described in Naba et al. (2015). Peptides were desalted using C18 Sep-Pak cartridges following manufacturer's instructions and dried by vacuum centrifugation. TMT labeling was performed according to the manufacturer's instructions. TMT-labeled samples were then pooled at a 1:1 ratio across all samples. The combined sample was vacuum centrifuged near to dryness and subjected to fractionation using an Agilent OFFGEL 3100 system. Resulting fractions were desalted on C18 StageTips (Rappsilber et al., 2007) and dried by vacuum centrifugation. Peptides were resuspended in 2% acetonitrile, 0.1% FA and injected in duplicate. Nano-flow separations were performed on a Dionex Ultimate 3000 RSLC nano UPLC system on-line connected with a Lumos Fusion Orbitrap Mass Spectrometer. A capillary precolumn (Acclaim Pepmap C18, 3 μm-100Å, 2 cm x 75μm ID) was used for sample trapping and cleaning. Analytical separations were performed at 250 nl/min over 90 min. biphasic gradients on a 50cm long capillary column. Acquisitions were performed through Top Speed Data-Dependent acquisition mode using a 2 seconds cycle time. First MS scans were acquired with at a resolution of 60'000 (at 200 m/z) and the most intense parent ions were selected and fragmented by High energy Collision Dissociation (HCD) with a Normalized Collision Energy (NCE) of 38% using an isolation window of 0.7 m/z. Fragmented ions were acquired with a resolution 50'000 (at 200m/z) and selected ions were then excluded for the following 60 s.

### Quantification and statistical analysis of ECM-enriched fraction proteomic data

RAW files were processed with Maxquant version 1.6.2.10 (Cox and Mann, 2008) and its search engine Andromeda against the Mus musculus complete proteome of Uniprot database (53449 sequences- release 07-2018), with the contaminants from Maxquant. Enzyme specificity was set to Trypsin and a minimum of seven amino acids was required for peptide identification. Up to two missed cleavages were allowed. A 1% FDR cut-off was fixed for the peptide and protein identifications. Carbamidomethylation (C) was set as a fixed modification, whereas oxidation (M), deamidation (N), Gln to pyro-Glu, hydroxylysine, hydroxyproline and Phospho (STY) were considered as variable modifications. Resulting text files from Maxquant were processed with in-house scripts in R (version 3.4.2; https://www.R-project.org/). Two steps of normalization were applied according to the corrected reporter intensities of the proteins

from the Extra-Cellular Matrix (ECM). These ECM proteins were defined as proteins belonging to different categories of the matrisome (http://matrisome.org; (Naba et al., 2016). The first step of normalization was the sample loading normalization (Plubell et al., 2017). Assuming that the total abundance of the proteins was equal across the TMT channels, the reporter ion intensities of all the spectra were summed and each channel was scaled according to this sum, so that the sum of reporter ion signals per channel equals the average of the signals across samples. The second step of normalization was the Trimmed M-Mean normalization with the package EdgeR (version 3.26.8; (Robinson et al., 2010). Assuming that the samples have a majority of proteins that are not differentially expressed, this step calculates normalization factors according to these presumed unchanged proteins. Proteins with high or low abundance and proteins with larger or smaller fold-changes were not taken into account. Differential protein expression analysis was performed using the R bioconductor package limma (version 3.34.9, 2018-02-22; (Ritchie et al., 2015), followed by the Benjamini-Hochberg multiple-testing method. Adjusted *P values* lower than 0.05 (FDR < 0.05) and absolute $\log_2$ fold-change > 1 were considered as significant. Differential protein expression analysis of the ECM related proteins was performed using the R bioconductor package limma.

### 16S analysis/16S rRNA gene amplicon sequencing

Cecal samples from the recolonization experiment collected for 16S rRNA sequencing were isolated using QIAamp DNA stool mini kit, following manufacturer's instructions. These samples were obtained 4-weeks post-recolonization. The 16S rRNA gene segment spanning the variable V4 region was amplified from DNA extracted from cecal contents samples using a multiplex approach with the barcoded forward fusion primer 5′-AATGATACGGCGACCACCGAGATCTACAC i5BARCODE TATGGTAATTGTGTGCCAGCM GCCGCGGTAA-3′ in combination with the reverse fusion primer 5′-CAAGCAGAAGACGGCATACGAGAT i7BARCODE AGTCAGT CAGCCGGACTACHVGGGTWTCTAAT-3′. One PCR reaction contained 0.25mM of each primer, KAPA HiFi Hot Start Ready Mix (Roche) and 20–100 μg of template DNA. PCR conditions were 98°6;C for 2min, followed by 25 cycles of 98°C for 30 s, 55°C for 30 s and 72°C for 20s and a final extension step at 72°C for 7min. Amplification of the V4 gene region was verified by electrophoresis on a 1.2% agarose gel. Reactions were purified using NucleoMag NGS clean-up beads (Macherey-Nagel) and were normalized using the SequalPrep Normalization Plate Kit (Invitrogen). Amplicons were pooled and concentration and quality were determined using the Qubit HS DNA kit (Invitrogen) and the Tapestation D1000 assay (Agilent), respectively. Amplicon sequencing was done on a MiSeq Benchtop DNA sequencer (Illumina) using a V2-500 cycle kit (Illumina Inc.). Using Dada2 (Callahan et al., 2016), phyloseq (Jacobs et al., 2013) and reshape2 packages (Baril et al., 2019) within R. Forward and reverse reads were trimmed to 230 and 210 bp, respectively, and chimeras were removed using the remove Bimera Denovo function. Taxonomy was assigned using custom databases containing the 16S rRNA gene sequences of all the bacterial species used in the gnotobiotic models. Amplicon sequence variants (ASVs) that were present at <0.5% were excluded.

### Intestinal contractility ex vivo

Spontaneous small intestinal muscle contractile activity was evaluated in a commercial organ bath. The entire small intestine was isolated and placed immediately in Krebs solution (118 mM NaCl, 4.7 mM KCl, 1.2 mM KH2PO4, 1.2 mM MgSO4.7H2O, 11.1 mM C6H12O6, 25 mM NaHCO3 and 2.5 mM CaCl2.2H2O in demineralised water) at 37 °C in 10cm petri dishes. The intestine was divided as follows: the Duodenum (Duo) is 5cm region post-pyloric sphincter, Jejunum (Jej) and Ileum (Ile) are determined as the proximal and distal half of small intestinal tissue downstream of the duodenum. Two longitudinal samples of approximately 1 cm each were dissected from the small intestine (centimeters ~6-7 for Duo-Jej samples and centimeters ~20-21 for the Jej-Ile samples). Strips of intestinal tissue were longitudinally suspended between a fixed holder and a force transducer (AD Instruments) in vessels of an organ bath (PL3508B6/25-220, Panlab, AD Instruments) containing 25mL Krebs solution at 37 °C and bubbling of carbogen (95 % O2 and 5 % CO2). A baseline tension of 1 g was set followed by a 1-hour equilibration period. Vessel buffers were changed at 20 minutes intervals throughout the experiment to maintain physiological osmolarity of the Krebs solution. The average tension, amplitude and frequency of spontaneous contractions were recorded over a 10 minutes period. The Parameters for the cycle detection settings were customised to include a smoothing window of 1 second and a normalising window of 2 second, the other parameters were left at their default settings. For samples where the first cycles detected by the software were not sinusoidal the sample was considered to no longer be healthy and was excluded from the analyses.

### Lamina propria cell isolation

For the leukocyte isolation from epithelial layer (intraepithelial lymphocytes - IELs) and from the lamina propria, the small intestine was divided from the upper to the distal part: 5 cm (duodenum), 15 cm (jejunum) and 15 cm (ileum). The upper jejunum (10 cm) was harvested, flushed with ice-cold 1x PBS and attached mesenteric tissue/fat and Peyer's Patches were removed. After opening the tissue longitudinally, small pieces of 1-2 cm were cut and transfer into epithelial cell removal solution (1x HBSS, 2% fetal calf serum inactivated (iFCS), 10 mM HEPES and 5 mM EDTA) and incubated on shaker at 37C for 20 minutes. Samples were washed 3-times with ice-cold 1x PBS to detachment of cells from epithelial cells and IELs through manual shaking of the tube. The washes were collected, spun down and snap frozen for RNA-seq of intestinal epithelial cell (IEC)-fraction, or after filtering in 70 m strainer, used for flow cytometry. The remaining tissue (lamina propria and muscularis layer) was minced prior to digestion in supplemented RPMI (Liberase TL 100 g/mL (Roche), DNAse I 10U/mL (Roche), 5% iFCS and 10 mM HEPES at 37C for 25 minutes. Digestion was deactivated using cold RPMI containing 10% iFCS and 10 mM HEPES at 1:1 ratio. The tissue was further dissociated by manual -

suction using serological pipette and filtered through 100 um cell strainer, spun down and washed twice with FACS buffer (1x PBS, 2% iFCS, 2 mM EDTA). The cells were used for Flow Cytometry, Flow Cytometry Sorting, Mass cytometry or RNAseq analysis.

### Flow cytometry and flow cytometry sorting

After isolation cells were washed and resuspended in FACS buffer (1x PBS, 2% iFCS, 2 mM EDTA) for counting using a Neubauer chamber in Trypan blue. 2-3 x$10^6$ cells were used for FACS staining. Single cell suspensions were incubated with viability dye (1:400) in 1x PBS for 20 min. After washing with FACS buffer, cells were incubated with FcR-block (1:100) for at 10 min and sequentially stained with the following surface antibody mixes: eosinophils – anti-CD45 (BV510, 1:200), siglec-F (BV605, 1:200), CD11b (FITC, 1:200), CD11c (PeCy7, 1:200), CD103 (PE,1:200), CD44 (BV421, 1:200), CCR3 (biotin, 1:200), Ly6C (AF700, 1:200), Gr1 (PerCP-Cy5.5, 1:200); monocytes-macrophages - anti-CD45 (V450, 1:200), CD3 (PerCP-Cy5.5, 1:200), CD19 (PerCP-Cy5.5, 1:200), Ly6G (PerCP-Cy5.5, 1:200), CD11b (FITC, 1:200), CD64 (AF647, 1:200), Ly6C (AF700, 1:200), I-A/I-E (BV510, 1:200). After washing, samples were fixed stained for 10 min with streptavidin, washed and fixed with 4% PFA for 30min and washed with FACS buffer before analysis using an LSRII and CANTO II Flow Cytometer (BD Bioscience). Data was analyzed using FlowJo software (Tree Star Inc.).

For FACS sorting eosinophils, cells were sorted on a FACSAria (BD Bioscience) as SSC-A$^{high}$, live, CD45$^+$ (V450, 1:200), MHCII$^-$ (BV510, 1:200), CD11b$^+$ (FITC, 1:200), siglec-F$^+$ (BV605, 1:200) and re-suspended in RPMI supplemented with 10% iFCS.

### Intestinal permeability (Ussing Chamber assay)

Segments of upper jejunum (2 cm) were removed and flushed with cold PBS. The segments were opened longitudinally and mounted between the halves of standard Ussing chambers. Once mounted, the tissues were bathed with Krebs buffer [NaCl (115 mM), $KH_2PO_4$ (2.0 mM), $MgCl_2$ (2.4 mM), $NaHCO_3$ (25.0 mM), KCl (8.0 mM), and $CaCl_2$, (1.3 mM), 10 mmol/litter (apical side) mannitol or glucose (basolateral side), pH 7.4] at 37 °C. Buffers were aerated and mixed by using a gas lift system (5% $CO_2$ and 95% $O_2$). Tissue responses were measured by clamping the potential difference (PD) to 0 mV by applying an Isc with a voltage-clamp apparatus (EVC-4000, World Precision Instruments, Sarasota, FL). After 20-30 min equilibration, 40 mL (100 mg/mL) of Fluorescein isothiocyanate (FITC)-dextran (4 kDa, Sigma) was added to the apical side of the chamber. Samples were taken in triplicate from the basolateral side immediately after FITC-dextran addition (baseline fluorescence) and every 10 min for 70 minutes and loaded in a 96-well plate (655077; Greiner Bio-One, Kremsmünster, Austria) kept in the dark for the entire duration of the experiment. Volume sampled from apical side was replaced with fresh Krebs solution. Fluorescence was measured using a VictorX4 2030 plate reader (Perkin-Elmer, Waltham, MA; excitation/emission: 488/520). Results are shown as relative fluorescence in the basolateral side compartment over time, normalized to individual baseline fluorescence.

### Transit time (Carmine Red assay)

The whole intestine transit time was measured with carmine red gavage. Mice were separated in individual cages and gavaged with 200 L of carmine red (6% w/vol., Sigma) diluted in 0.5% methylcellulose (Sigma). The time at which gavage took place was recorded as $T_0$. After gavage, fecal pellets were monitored at 10 min intervals for the presence of carmine red. Total GI transit time was considered as the interval between T0 and the time of first observance of carmine red in stool.

### Bacterial flow cytometry

*Akkermansia muciniphila* YL44 (DSM 26127) was cultured for 48 hours in sterile Brain-Heart Infusion (BHI) broth supplemented with 0.25 g/L autoclaved Type II gastric mucin (Sigma) under anaerobic atmosphere (10% $H_2$, 10% $CO_2$ and 80% $N_2$) in a Whitley A95 incubator. The culture was centrifuged for 10min at 3,000g, washed twice and re-suspended in sterile-filtered PBS/2%BSA/0.02% sodium azide and diluted to ~$10^7$ bacteria/ml (OD595 0.1 = $10^8$ bacteria/ml). Serum was diluted 1:10 in PBS/2%BSA/0.02% sodium azide, heat-inactivated at 56°6;C for 30min and centrifuged at 16,000 g for 5min at 4°6;C to remove any bacteria sized contaminants. This serum supernatant was used to perform serial dilutions. 2.5x$10^5$ bacteria were added to each well and incubated with the serial dilutions of serum for 1 h at 4°6;C, centrifuged for 10min at 3,000 g, washed twice and then re-suspended in 1:50 anti-IgG1 (APC), -IgG2b (BV711), -IgG2c (BV421), -IgG3 (BV605) and –IgM (PE) and incubated overnight at 4°6;C. The bacteria were washed twice in PBS/2%BSA/0.02% sodium azide and then re-suspended in PBS/2%BSA/0.02% sodium azide and acquired on a FACS Canto (BD) using FSC (forward scatter) and SSc (side scatter) in logarithmic mode. Bacterial culture without serum and serum from YL44-intravenous injected mice were used as negative and positive staining control, respectively. Data was analyzed using FlowJo software (Tree Star Inc.).

### Immunoglobulin electrochemiluminescence immunoassay

Total concentration of IgG1, IgG2a, IgG2b, IgG3 and IgM in serum were determined using the Mouse Isotyping Panel 1 kit according to manufacturer's instructions (Meso Scale Discovery).

### Shotgun Proteomics Whole Protein Dimethylation and Mass Spectrometry (MS)

Segments from the upper jejunum (2 cm) from GF and colonised mice were surgically removed and protein lysates were obtained by tissue lysis in buffer containing 1% SDS, 0.1 M DTT in 200 mM HEPES (pH 8.0) and cOmplete™ Protease Inhibitor Cocktail (MilliporeSigma, Oakville, ON, Canada). Samples were reduced with 10 mM dithiothreitol (DTT) for 1 h at 55 °C. Once cooled at room temperature (RT), cysteine alkylation was achieved by incubation with a final concentration of 15 mM iodoacetamide for

Please cite this article in press as: Ignacio et al., Small intestinal resident eosinophils maintain gut homeostasis following microbial colonization, Immunity (2022), https://doi.org/10.1016/j.immuni.2022.05.014



25 min in the dark at RT. Next, samples were precipitated in acetone/methanol, washed three times in methanol, and trypsinized (Trypsin Gold from Promega, Madison, WI, USA). The pH was adjusted to 6.0 with HCl. To label peptide α- and ε-amines, samples were incubated for 18 h at 37 °C with isotopically heavy [40 mM 13CD2O + 20 mM NaBH3CN (sodium cyanoborohydride)] or light labels [40 mM light formaldehyde (CH2O) + 20 mM NaBH3CN]. Next, samples were combined and subjected to C18 chromatography before being run on liquid chromatography and tandem mass spectrometry.

### High-Performance Liquid Chromatography (HPLC) and Mass Spectrometry (MS) (Germ-free and colonised mice experiments)

The liquid chromatography and mass spectrometry experiments performed with upper jejunum samples from GF and colonised mice were carried out by the Southern Alberta Mass Spectrometry (SAMS) core facility at the University of Calgary, Canada. The analysis was performed on an Orbitrap Fusion Lumos Tribrid mass spectrometer (Thermo Scientific) operated with Xcalibur (version 4.0.21.10) and coupled to a Thermo Scientific Easy-nLC (nanoflow liquid chromatography) 1200 system. Tryptic peptides (2 μg) were loaded onto a C18 column (75 μm × 2 cm; Acclaim PepMap 100, P/N 164946; Thermo Scientific) at a flow rate of 2 μL/min of solvent A (0.1% formic acid and 3% acetonitrile in LC-MS grade water). Peptides were then electrosprayed using 2.3 kV voltage into the ion transfer tube (300 °C) of the Orbitrap Lumos operating in the positive mode. The Orbitrap first performed a full MS scan at a resolution of 120,000 fwhm to detect the precursor ion having a m/z between 375 and 1,575 and a +2 to +7 charge. The Orbitrap AGC (Auto Gain Control) and the maximum injection time were set at 4 × 105 and 50 ms, respectively. The Orbitrap was operated using the top speed mode with a 3 s cycle time for precursor selection. The most intense precursor ions presenting a peptidic isotopic profile and having an intensity threshold of at least 5,000 were isolated using the quadrupole and fragmented with HCD (30% collision energy) in the ion routing multipole. The fragment ions (MS2) were analyzed in the ion trap at a rapid scan rate. The AGC and the maximum injection time were set at 1 × 104 and 35 ms, respectively, for the ion trap. Dynamic exclusion was enabled for 45 s to avoid the acquisition of the same precursor ion having a similar m/z (±10 ppm).

### Proteomic Data and Bioinformatics Analysis (Germ-free and colonised mice experiments)

Spectral data were matched to peptide sequences in the murine UniProt protein database using the Andromeda algorithm (Cox et al., 2011) as implemented in the MaxQuant (Cox and Mann, 2008) software package v.1.6.0.1, at a peptide-spectrum match FDR of <0.01. Search parameters included a mass tolerance of 20 ppm for the parent ion, 0.5 Da for the fragment ion, carbamidomethylation of cysteine residues (+57.021464 Da), variable N-terminal modification by acetylation (+42.010565 Da), and variable methionine oxidation (+15.994915 Da). N-Terminal and lysine heavy (+34.063116 Da) and light (+28.031300 Da) dimethylation were defined as labels for relative quantification. The cleavage site specificity was set to Trypsin/P, with up to two missed cleavages allowed. Significant outlier cutoff values were determined after log(2) transformation by box-and-whisker analysis using the BoxPlotR tool (doi: 10.1038/nmeth.281). A minimum of two distinct peptides per protein for the quantification was used.

### Detection of proliferating cells with anti-BrdU

BrDU was dissolved in sterile PBS at a concentration of 10 mg/mL and filtered through 0.2 μm pore filter. An initial dose of 1 mg BrDU were intraperitoneally injected and mice were given 0.8 mg BrDU/mL supplemented in the drinking water for 8 days. The drinking water was prepared at 0.8-1 mg/mL sterile water and renewed every other day. After isolation of lamina propria cells, 2-3 x106 single cell suspension were incubated with viability dye (1:400) in 1x PBS for 20 min. Cells were washed with FACS buffer and incubated with FcR-block (1:100) for at 10 min and sequentially stained with the surface antibodies anti-siglecF (PE, 1:100) and –CD11b (APC-Cy7, 1:100) for 25min on ice. Cells were washed with FACS buffer and subsequently fixed and permeabilized with Cytofix/Cytoperm buffer (BD) for 15min. After washing with Perm/Wash Buffer (BD) cells were stained with anti-BrDU (PerCP-Cy5.5, 1:30) for 20min at room temperature. The cells were washed again in Perm/Wash Buffer and stored in FACS buffer at 4 °C before acquisition at LSRII flow cytometer (BD).

### Transmission Electron Microscopy (TEM)

After dissection, the tissue was fixed in 0.15M HEPES containing 2.5% glutaraldehyde (Agar Scientific, Stansted, Essex, UK) (709 mOsm, pH 7.34) for 24 hours at 4 °C. Samples were washed twice with 0.15M HEPES for five minutes and re-fixed with 1% OsO4 (SPI Supplies, West Chester, USA) in 0.1M Na-cacodylate-buffer (Merck, Darmstadt, Germany) at 4C for one hour followed by three washes in 0.05M maleate-NaOH buffer (Sigma, Darmstadt, Germany). Samples were then block-stained 4 °C in 0.05M maleate-NaOH buffer containing 0.5% uranyl acetate (Fluka, Buchs, Switzerland) for one hour. Samples were washed three times for five minutes in 0.05M maleate-NaOH buffer and dehydrated in 70%, 80%, and 96% ethanol for 15 min each, at room temperature. Subsequently, samples were immersed in 100% ethanol three times for 10 min, in acetone (Merck, Darmstadt, Germany) two times for 10 min, and finally in acetone-epon (1:1) overnight at room temperature. The next day, samples were embedded in epon (Sigma) and left to harden at 60 °C for five days. Sections were produced with an ultramicrotome UC6 (Leica Microsystems, Vienna, Austria). Firstly, semi-thin sections of 1μm were stained in 0.5% toluidine blue (Sigma) for light microscopy. Ultrathin sections (70-80nm) were mounted on single slot copper grids and stained with uranyl acetate and lead citrate with an ultrostainer (Leica Microsystems, Vienna, Austria). Sections were examined with a transmission electron microscope (CM12, Philips, Eindhoven) equipped with a digital camera (Morada, Soft Imaging System, Münster, Germany) and image analysis software (iTEM).

### Degranulation of Eosinophil Peroxidase (EPO)

Small intestine sorted-eosinophils from germ-free and SPF colonised mice were re-suspended on RPMI 1640 without phenol red, and 5-10x105 cells/well were plated in 100 mL. Total EPO was measured on eosinophils lysed in 0.2% SDS normalized by intact eosinophils on the presence of 100 μL o-phenylenediamine reagent (800 μL 5 mM o-phenylenediamine in 4 mL 1M Tris [pH 8], 5.2 mL H2O, and 1.25 μL 30% $H_2O_2$). The reaction was terminated by the addition of 100 μL 4 M $H_2SO_4$ to each well and read at 492 nm.

### Mass Cytometry (CyTOF) Staining and Acquisition

Purified unconjugated antibodies custom-made with no additional protein carrier from Biolegend or Thermo Fisher. CyTOF antibodies were labeled with metal-tag using the MaxPar Antibody Labeling kit (Fluidigm). A total of $3x10^6$ cells from the upper jejunum were incubated in FcR-block (1:100), followed by incubation with surface marker staining cocktail for 30 min at 4°C. For viability staining, cells were washed with PBS and incubated for 5 min in room temperature in 200 μl of 1 μM cisplatin solution (BioVision). Cisplatin was quenched by adding 2 ml of 5% serum-containing PBS. For iridium labeling of cellular DNA, cells were suspended in 1 ml of 100 nM of iridium (Fluidigm) in PBS containing 0.3% saponin and 1.6% formaldehyde for 1 h at 4 °C. Cells were then washed and kept in PBS with 1.6% formaldehyde in 4°C for 1 to 4 days before acquisition. Immediately prior data acquisition, cells were pelleted in Milli-Q water. cCells were then re-suspended into 1 ml of EQ beads (Fluidigm) diluted 1:10 in Maxpar Cell Acquisition Solution (Fluidigm) and filtered through cell strainer cap tubes. Cells were acquired at rate of 100–250 events per second on a third-generation Helios mass cytometer (Fluidigm).

### CyTOF Analysis

Acquired raw FCS files were normalized with the preloaded normalizer algorithm on CyTOF software version 6.7. Normalized CyTOF FCS files were manually pre-gated on singlets ($^{191}Ir^+$ $^{193}Ir^+$) viable ($^{195}Pt^-$) CD45 (89Y) on FlowJo and exported to downstream analysis. Downstream analysis was performed using the R package diffcyt. Briefly, the fcs files were read in as a flowset. An arcsinh transformation was used with a cofactor of 5. FLOWSOM was used for clustering and UMAP (default parameters) for dimension reduction and visualization. For differential abundance analysis, we used diffcyt-DA-edgeR and diffcyt-DS-limma for differential expression analysis (Nowicka et al., 2017).

### Bone Marrow-Derived Eosinophil (BMEo) Culture

Bone marrow cells were isolated from GF BALB/cJ mice. Bones were harvested and flushed with sterile 1x PBS and red blood cells were lysed with ACK Lysis Buffer. $2x10^6$ cells/mL were cultivated in IMDM with Glutamax (Life Technologies, Invitrogen) supplemented with 20% iFCS, 100 U ml–1 penicillin–streptomycin, 100 ng/ml stem cell factor (SCF; PeproTech) and 100 ng/ml FLT3 ligand (FLT3-L; PeproTech) from days 0 to 4. On day 4, the medium containing SCF and FLT3-L was replaced with fresh medium containing 10 ng/ml recombinant mouse (rm) IL-5 (PeproTech) only. On day 8, cells were transferred to a new flask at density of $1x10^6$ cells/mL maintained in new media containing rmIL-5. From this point forward, every other day one-half of the medium was replaced with fresh medium containing rmIL-5. On day 14, eosinophils were purified by anti-Siglec-F MACS beads separation (Miltenyi Biotec) and 10-12 x $10^6$ BMEo were intravenously transferred into dbl.GATA1 mice. Cells were transferred once a week for a total of 4 weeks. 50,000 BMEo were subjected to flow cytometry and cytospin (Thermo Shandon) for phenotype analysis. The cytospin preparations were fixed and stained using a modified Giemsa preparation (Diff Quik).

### Bomb Calorimetry (Indirect calorimetry)

Mice were individually housed and acclimatized for 24h on Type 2IVC cages with a grid floor. On the day of analysis, 3-5 hours after fasting, the mice were given *ad libidum* access to food and water over the course of 24 hours. After 24 hours, mice were placed back in groups in their home cages on normal racks in the animal facility. Food consumption was assessed, by food weighting and the feces are collected (from 24 hours period) for measurement of their energy content using an IKA C200 Bomb calorimeter. Fecal pellets were desiccated and pre-weight prior to combustion.

### Triglyceride Analysis

Blood was collected 1 day prior the experiment (T0 – baseline tg level) from the tail vein of all mice after fasting for 3 hours. On the day of the experiment, the mice were fasted for 3 hours prior to intra-gastric gavage with 200μl of olive oil (Sigma). Blood was collected from the tail vein (stored in EDTA tubes) at 1-, 2- and 3-hours post-gavage. The samples were then snap frozen in liquid nitrogen until analysis. Plasma concentrations of triglycerides were determined using the Cobas C111 robot (Roche Diagnostics).

### High-fat diet experiment

Mice were co-housed and their weights measures at timepoint-0 (T0) weekly until 9-15 weeks into the experiment. To measure body composition (fat vs. protein), mice were analyzed using EchoMRI-100 (EchoMRITM) every 3 weeks with the fat mass calculated and normalized based on their weight within the given time point. Weight gain over time was calculated as the fold change from the initial weight at T0. HFD and control-chow was obtained from ResearchDiets (USA).

Please cite this article in press as: Ignacio et al., Small intestinal resident eosinophils maintain gut homeostasis following microbial colonization, Immunity (2022), https://doi.org/10.1016/j.immuni.2022.05.014



### Intestinal fluid collection

Intestines were dissected and small intestinal contents flushes out with 5mL of ice-cold intestinal wash buffer (10%vol 0.5M EDTA, 10%vol 10xPBS, 10%vol dd$H_20$ and 10mg (per 100mL) soybean trypsin inhibitor (Sigma T9128-1G) into a tube containing 40μL phenylmethylsulfonylflouride (PMSF). The tube was briefly vortexed and stored on ice until all mice were dissected. The intestinal wash sample was centrifuged at 3200xg for 15 minutes at 4C and afterwards aliquoted into 3-4 2mL tubes. Samples were stored at -80 °C to prevent protein degradation. When lamina propria preparations were prepared from the same small intestine, the intestine was flushed with 4mL DPBS into 1 mL of 5x concentrated intestinal wash buffer.

### IgA ELISA

Protein-absorbing ELISA plates (Nunc) were coated with 1 μg/mL goat anti-mouse IgA (Southern Biotechnologies) in 0.1M $NaHCO_3$ overnight at 4 °C. Plates were washed in 0.05% Tween20 in PBS and blocked with 2.5% weight per volume (w/v) bovine serum albumin (BSA) in PBS for two hours at room temperature. The blocking solution was then discarded, and pre-diluted serum or neat intestinal wash samples added and serially diluted across the plate. For each plate, a standard isotype for IgA with initial concentration of 2000 ng/mL was serially diluted to obtain a standard curve. Samples were incubated for two hours at room temperature. For detection, horseradish peroxidase (HRP)-conjugated anti-mouse IgA (Sigma, 1/1000 dilution) was added for one hour at room temperature and reaction was developed with 0.05% $H_2O_2$ in 0.1M $NaH_2PO_4$ containing 0.1 mg/mL ABTS peroxidase solution. Colorimetric reaction was read at 415 nm with microplate reader (Bio-Rad). Standard curves and antibody concentrations were analyzed with Microplate Manager III software (Bio-Rad).

## QUANTIFICATION AND STATISTICAL ANALYSIS

Numbers of replicates and experiments and statistical tests for each experiment are indicated in in the respective figure legends. For statistical analysis, data were analyzed by GraphPad Prism. Unpaired Student's t test, two-way ANOVA with Tukey's multiple comparisons post-test, or Mann-Whitney test were used for statistical analysis as indicated in figure legends. Correlation analysis was performed by Spearman nonparametric test. Error bars represent standard deviation (SD). $p < 0.05$ was considered significant.